Dynamic Interfacial Tensions and Dilatational Viscoelastic Properties of Asphaltenes at Oil/Water Interface at High Pressure and High Temperature Conditions

By

Meng Luo

A thesis submitted in partial fulfillment of requirements for the degree of

Master of Science

In

Chemical Engineering

Department of Chemical and Material Engineering

University of Alberta

Abstract

The dynamic interfacial tension and dilatational viscoelasticity behaviors of asphaltenes at oil/water interfaces were investigated by means of an oscillating droplet tensiometer. This oscillating droplet tensiometer was modified to handle temperature of 120 °C and pressure up to 700 kPa. For dynamic interfacial tension, the effect of temperature, addition of artificial surfactants and aromaticity of solvent were investigated. It was found that increasing temperature, addition of surfactant and decreasing the aromaticity of the solvent could decrease the dynamic interfacial tension and accelerated the diffusion rate of asphaltenes migrating to the oil/water interface. It was also found that the adsorption kinetics of asphaltenes at oil/water interface can be categorized into three regimes where the Regime I is the fast diffusion-controlled process and Regime III is the slow adsorption-controlled process with the Regime II being the transitional stage in between. For interfacial dilatational behavior, the effect of temperature for pure toluene/water system, temperature with asphaltenes at toluene/water system, concentration of asphaltenes and salinity of aqueous solution were investigated. It was found that increasing temperature of pure toluene/water or asphaltenes in toluene/water system can reduce the elastic modulus significantly at different oscillating frequencies from 0.1 to 1 Hz. In addition, concentrated asphaltene solutions at oil/water phase have shown reduced elastic moduli and decreasing significantly if the frequency increased. Finally, as the salinity of aqueous solution increased, the elastic moduli increased as the interface became more rigid. These phenomena reveal the general trend in emulsion treating and oil recovery in various industrial processes.

Preface

For the work of Chapter 3 and 4, I was responsible for designing and conducting the experiments, data fitting and interpretation, as well as writing of the manuscripts. Dr. Hongbo Zeng offered great guidance on the direction of research and the revision of the thesis.

Acknowledgement

For the long journey of my graduate study, I would like to sincerely thank my supervisor Dr. Hongbo Zeng. Not only he coached me through the scientific research but also help me with my program with great patience. I would like to also thank to Lily Laser from Graduate Student Services, who help me through entering the program and guide me from the very start.

Also, I would like to thank Dr. Ling Zhang and Dr. Duo Wang for their support of case histories, background knowledge and technical guidance.

Finally, I would like to thank my family members to their financial and emotional support.

Contents

List of Tables

List of Figures

List of Symbols

J	Joule
N	Newton
Da	Dalton (unified atomic mass unit)
t	Time
Γ_t	Surface excess concentration
D	Diffusion coefficient
C_0	Bulk concentration
γ	Interfacial tension
R	Gas constant
T	Temperature (Kelvin)
k	Slope in plot
γ_{eq}	Equilibrium interfacial tension
E	Surface elasticity
$\Delta\gamma$	Surface tension difference
E’	Elastic modulus
E”	Viscous modulus

List of Acronyms

SAGD	Steam-assisted Gravity Drainage
CMC	Critical Micelle Concentration
CNAC	Critical Nanoaggregation Concentration
CCC	Critical Clustering Concentration
CCD	Charge-coupled device
IFT	Interfacial tension
PFA	Perfluoroalkoxy alkane
PEG-PPG-PEG	Poly (ethylene glycol)-block-poly (propylene glycol)-block-poly (ethylene glycol)
L-64	Pluronic® L-64 surfactant
NPT	National Pipe Thread
CAS	Chemical Abstract Service
ASTM	American Society for Testing and Materials
FWKO	Free Water Knock Out

Chapter 1 Introduction

1.1 Background Information

Steam-assisted gravity drainage (SAGD) is a thermally enhanced oil recovery technique in which a large quantity of steam is continuously injected to extract heavy oil or bitumen from underground formation. Typical steam to oil ratio is around 3 barrel of water and 1 production of bitumen. Due to extreme temperature and agitation during the extraction process, complex water-in-oil-in-water emulsion is created [1]. Compared to traditional surface mining and other enhanced thermal recovery techniques, SAGD has its own advantages and disadvantages: land disturbance is far less an issue for SAGD, its elevated temperature translates to higher extraction rate, and much reduced water treating costs. One major drawback when dealing with SAGD emulsions is the high viscosity of the resulting bitumen (100 – 1,000,000 mPa.S at room temperature) and similar density to water, which makes more difficult for its transportation and separation from water [2].

A diluent is usually added to reduce the density and viscosity of heavy oil and bitumen. The reduced density and viscosity help water/oil separation and ease of transportation [3]. Percentage of the diluent addition, composition of the diluent and surfactants present in the diluent will affect the emulsion stability and may cause the dehydration of the water from oil phase more difficult. These stable emulsions are highly undesirable because they can cause several problems such as off-specification crude oils, corrosion in pipes and catalyst poisoning in subsequent crude oil processes. Treating these complex emulsions is technically challenging and economically unfavorable because of their high stability. Most of the times, chemicals such as emulsion-breaking chemistries are required.

Some researchers believe that emulsion stability depending on the irreversible adsorption of asphaltenes at oil-water interface combining with other natural materials containing resins, clays, and naphthenic acid etc. [4, 5]. Asphaltenes are complex aromatic fused rings with aliphatic side chains which soluble in aromatic solvents such as toluene and xylene but insoluble in aliphatic solvent such as pentane, hexane, and heptane [6, 7]. Asphaltenes have typical molecular weight in the range of 400 Da to 1000 Da and consist of aromatic hydrocarbon rings with peripheral aliphatic chains, containing heteroatoms such as nitrogen, oxygen and sulphur as well as metal elements such as vanadium, nickel and iron [8,9]. Due to their complex composition of asphaltenes, pinpointing a defined structure is often difficult. For the past years, two major theories on asphaltenes structures are *archipelago* and *island* model. However, with improvement of analytical techniques, island model is more accepted [10]. The island model supports the molecular weights and aromatic fused rings structures of asphaltenes from various sources [11].

1.2 Asphaltenes aggregation behaviors

The most interesting characteristics of asphaltenes is the aggregation behavior. Decades ago, while the understanding of asphaltenes behaviors at its initial stage, the surface active asphaltenes were considered as surfactants. Similar to surfactants in aqueous solution, critical micelle concentration (CMC) was used to describe the asphaltenes aggregation behaviors. The CMC ranges were determined with types of asphaltenes and solvents used and then empirically fitted to Flory-Huggins interaction parameters [12]. However, CMC theory fails to describe the aggregation behavior of asphaltenes and surfactants. It was observed that micelles formation occurs when the concentration of surfactants is above CMC with aggregation number from 50 ~ 100 molecules for a typical surfactant in aqueous solution [13]. CMC cannot be determined if the aggregation number is less than 50. As the structure and aggregation number difference between asphaltenes and

surfactant, CMC was not able to describe the aggregation behavior of asphaltenes. Instead, critical nanoaggregation concentration (CNAC) and critical clustering concentration (CCC) began to be accepted widely with Yen-Mullins model [10]. Yen-Mullins model specified that the most probable asphaltenes is island molecular architecture. Asphaltenes form nanoaggregates with an aggregation number less than 10 with sufficient concentration. At higher CCC concentration, asphaltenes nanoaggregates further form clusters with relatively small aggregation numbers. The CNAC is generally measured as 50 – 100 mg/L or sometimes as low as 20 – 50 mg/L depending on the sources of asphaltenes. Stacking of asphaltenes through π-π interaction between polyaromatic planes also contributes to the formation of nanoaggregates. Several factors were contributed to asphaltenes aggregation: concentration of bulk solution, sources of asphaltenes, system temperature and aromaticity of the solvent [11-13].

1.3 Interfacial Tension Studies

The interfacial tension is defined as the work which must be done to increase the area of the interface between two adjacent phases which do not mix completely with one another [14]. The term relates to the liquid/liquid and liquid/solid phase boundaries. The proportionality factor γ is to describe surface tension as well as IFT. Energy per unit area (J/m^2) and force per unit length (N/m) are used to quantify surface tension or IFT. According to the physical meaning, surface tension of IFT is a two-dimensional factor associated with energy.

IFT between the aqueous phase and the organic phase with addition of asphaltenes has been studied by numerous researchers to reveal the adsorption behavior of asphaltenes at the oil/water interface. Effect of aging time, asphaltenes concentration, and types of solvent, pH effect of aqueous phase,

salinity of aqueous phase, temperature and pressure are the most focused aspects in asphaltene IFT studies [15 - 20].

The effect of temperature and pressure on the interfacial tension for pure solvent system has been studied long time ago. The effect of the pressure on interfacial tension for various solvents was minimal compared to that of temperature [21]. With less than 200 atmospheric pressure, there is no significant change in IFT. However, with temperature increase from 25 °C to 100 °C, significant decrease of IFT was observed. With the maximum SAGD surface processing facility operating pressure less than 15 atmospheric pressure, the effect of pressure will be ignored for this study.

For asphaltenes in organic solvent with water system, with increasing aging time, more asphaltenes molecules adsorb to the oil/water interface which leads to gradual decrease of IFT. Compared to surfactants, asphaltenes has larger molecular weight and are less surface active, it is much more difficult for asphaltenes to reach a steady state. The time reaching to the equilibrium could be a number of hours [18]. From the studies of aging time, the adsorption process for asphaltenes is a slow process compared to surfactant reconfiguration. The equilibrium IFT for asphaltenes was empirically obtained.

The diluent used to reduce the density and viscosity of the bitumen come from different sources and their composition varies greatly. As the ratio of aromatic to aliphatic components varies, the aromaticity of the organic phase is important. One study found that as the volume percentage of the aliphatic solvent increases, the IFT shows increasing trend gradually [22]. However, for this set of experiment, the results shown as the composition of aliphatic solvent increases, the IFT decreases even though the samples are different. Asphaltenes dissolved in “good solvent” like toluene will reach equilibrium faster than “poor solvent” such as pentane and heptane at higher

concentrations. Except the adsorption time, the effect of the solvent also correlates to the emulsion stability. The emulsion stability has been reported that with the increasing heptane volume percentage, the stability increases at first and reached a peak, and finally decreases. For this study, the solvent effect of toluene versus heptane combination was investigated.

In Athabasca oil sands, it is generally believed that the bitumen surrounded by hydrophilic water films and then the bitumen can be extracted by aqueous solution [23]. However, in this watery layer, it also contains salt accumulated from the formation. During the extraction process, the emulsified water contains salt is present in the oil phase. It is crucial to investigate the impact of salt (mostly in form of monovalent chloride salt) to the IFT between oil/water interface. With increasing concentration of potassium chloride, the IFT of crude oil system was found to decrease slightly within a low salinity range and increase afterwards. It was proved that the existence of potassium chloride would negatively affect the oil recovery [24].

It is important to study the adsorption kinetics of asphaltenes at the oil/water interface at elevated temperature since at SAGD field, above 200 °C of steam was used to extract bitumen from underground. Once reached to the surface processing facility, the temperature is lowered to 120 ~ 130 °C. One study found that there was no significant influence on adsorption in the range of 5 °C to 45 °C for asphaltenes extracted from Brazilian crude oils [25]. Other study shows that IFT and elastic moduli at oil/water interface shown little relevance with temperature varying from 23 °C to 60 °C. In this study, higher temperature (above 100 °C) was used to study adsorption kinetics of asphaltenes at different temperatures.

1.4 Interfacial dilatational rheology studies

Rheology describes the deformation and flow behavior of a solid or liquid. Interfacial rheology describes the viscoelastic properties at the interface between two immiscible liquids (or gas/liquid interface). For petroleum industries, the interfacial rheology between the oil and water interface has been linked to the emulsion stability. Interfacial rheology describes the relationships between IFT and deformation of the interface as a function of time during an oscillation process [26]. Interfacial rheology provides more insight into a dynamic system simulation in the petroleum chemical processes. In the surface processing facility of SAGD plant, hence, in free water knockout vessel (FWKO), where complex oil-water emulsions are treated, the expansion and contraction of the interface between the oil/water under low mechanical agitation can be simulated with interfacial rheological experiments. Dilatational and shear deformation are the two main types of deformations of interfacial rheology. For dilatational deformation, the shape of the interface is constant, and the interfacial area increases and decreases with oscillation with time. For shear deformation, the interfacial area remains steady while the shape of the interface is altered. The reformation and interaction of two phases with adsorbed asphaltene molecules can be studied with different conditions. Effects of aging time, frequency of oscillation, concentrations of asphaltenes, pH value of the aqueous phase, salinity of the aqueous phase, aromaticity of solvents, and presence of surfactants on the interfacial dilatational rheology studies have been reported by many researchers [27].

Elastic and viscous moduli are the most important parameters describing the behaviors of interfacial elasticities. It was observed that enhancement of elastic modulus and viscous modulus was observed with the increasing aging time and a plateau was reached at the end of the

experiments [28]. The everchanging IFT and dilatational moduli indicate intermolecular cross-linking and aggregation of asphaltene molecules at oil/water interface.

Frequency sweeps are usually used to determine the interfacial dilatational rheology. At low frequency, the freshly exposed asphaltenes are able to migrate to the oil/water interface within allowable amount of time during each cycle. Therefore, the diffusion controlled process dominates at lower frequency. However, there is little time to allow asphaltenes travel to the oil/water interface at high oscillation frequencies, the measured elastic moduli are equal to instantaneous moduli. Therefore, the elastic moduli are amplified by increase oscillation frequencies [29].

Considering interfacial rheology studies of the salt effect (mostly sodium chloride) on the oil/water system was investigated by Alves [30]. It showed that both elastic and viscous modulus of interfacial elasticity were always increased with the increased concentration of sodium chloride in the aqueous phase. Our results have shown similar results at 120 °C.

1.5 Objectives

The objective of this thesis is to investigate the relationships of dynamic interfacial tensions and interfacial dilatational behaviors of asphaltenes present in the oil/water interface under various conditions. The instrument used for this study is a modified high pressure high temperature pendant drop shape goniometer. By measuring the drop shape factor, the dynamic IFT and dilatational moduli are calculated and recorded. For adsorption kinetics, the effect of temperature is first investigated. Moreover, the effects of addition of surfactants at different temperature are examined as well. And then, the effect of aromaticity of solvent system were examined as well for studying the adsorption kinetics.

For interfacial dilatational rheology studies, the pure toluene/water system at various temperature is used to establish the baseline. Then the asphaltenes containing toluene drop is measured in the bulk water system at different temperature to investigate the change in elastic and viscous moduli. At very challenging condition of 120 °C, different concentrations of asphaltenes toluene solution are evaluated for interfacial dilatational properties. Finally, the asphaltenes/toluene droplet in different concentrations of sodium chloride solutions are tested at 120 °C to evaluate the general trend of elastic and viscous moduli. All these evidences are the related to emulsion stability and oil recovery in the real industry application.

1.6 Outlines of this thesis

Chapter 1 introduces the background information about asphaltene, its structure and molecular weights and its aggregation behaviors. In this chapter, the current stage of research on IFT and interfacial dilatational rheology were also reviewed.

Chapter 2 explains the techniques used to measure the dynamic IFT and interfacial dilatational rheology at high pressures and high temperatures.

Chapter 3 investigates the effect of temperature on dynamic IFT for asphaltenes at toluene/water interface. Effect of addition of artificial surfactants competing with asphaltenes at toluene/water interface at different temperatures. At last, the effect of solvent comprised of toluene/heptane was used to examine the adsorption kinetics.

Chapter 4 investigates the interfacial dilatational rheology for various conditions. First, the pure toluene/water system was investigated from 30 °C ~ 120 °C under 350 kPa of pressure as the baseline. Then the effect of temperature on interfacial dilatational properties were investigated for asphaltenes in toluene/water interface. Again, at 120 °C, the different concentrations of asphaltenes

solutions were scanned for general trend. Finally, the effect of salinity (sodium chloride) on elastic and viscous moduli were shown.

Chapter 5 summarizes the major conclusions for this thesis. Also, future directions and possible improvement on instruments and techniques are discussed.

Reference

(1) Acosta, E. "Achieving sustainable, optimal SAGD operations." *Journal of Petroleum Technology***,** 62 (11), 24 – 28.

(2) Saniere, A.; Henaut, I.; Argillier, J. "Pipeline transportation of heavy oils, a strategic, economic and technological challenge." *Oil & Gas Science and Technology.* **2004,** 59, 455 – 466.

(3) Wu, X. A.; Czarnecki, J. "Modeling diluted bitumen-water interfacial compositions using a thermodynamic approach." *Energy & Fuels.* **2005,** 19 (4), 1353 – 1359.

(4) McLean, J. D.; Kilpatrick, P.K. "Effect of asphaltene aggregation in model-toluene mixtures on stability of water-in-oil emulsions." *J. Colloid Interface Sci.* **1997**, 196, 23 – 24.

(5) Yarranton, H. W.; Sztukowski, D. M.; Urrutia, P. "Effect of interfacial rheology on model emulsion coalescence: I. Interfacial rheology." *J. Colloid Interface Sci.* **2007**, 310 (1), 246 – 252.

(6) Kilpatrick, P. K. "Water-in-crude oil emulsion stabilization: review and unanswered questions." *Energy & Fuels.* **2012,** 26 (7), 4017 – 4026.

(7) Adams, J. J. "Asphaltene adsorption, a literature review." *Energy & Fuels,* **2014,** 28 (5), 2831 – 2856

(8) Speight, J. G. "*The chemistry and technology of petroleum*." 3rd ed. Marcel Dekker, New York, **1999;** p xiv, 918p

(9) Mullins, O. C. "*Asphaltenes, heavy oils, and petroleomics."* Springer: New York, **2007;** p xxi, 669p

(10) Mullins, O. C.; Sabbah, H.; Eyssautier, J.; Pomerantz, A. E.; Barre, L.; Andrews, B.; Ruiz-Morales, Y. et al. "Advances in asphaltene science and the Yen-Mullins model." *Energy & Fuels, **2012***, 26 (7), 3986 – 4003.

(11) Groenzin, H.; Mullins, O. C. "Molecular size and structure of asphaltenes from various sources." *Energy & Fuels*, **2000**, 14 (3), 677 – 684.

(12) Rogel, E.; Leon, O.; Torres, G.; Espidel, J. "Aggregation of asphaltenes in organic solvents using surface tension measurements." *Fuel,* **2000,** 79 (11), 1389 – 1394.

(13) Masliyah, J. H.; Czarnecki, J. A.; Xu, Z. "*Handbook on theory and practice of bitumen recovery from Athabasca Oil Sands, Vol I and II."* University of Alberta Press, Edmonton, AB, **2011.**

(14) Butt, H.; Graf, K.; Kappl, M. "*Physics and chemistries of interfaces."* Wiley. p. 32.

(15) Sheu, E. Y.; Storm, D. A.; Shields, M. B. "Adsorption kinetics of asphaltenes at toluene/acid solution interface." *Fuel,* **1995**, 74 (10), 1475 – 1479.

(16) Hu, C.; Garcia, N. C.; Xu, R.; Cao, T; Yen, A.; Garner, S. A.; Macias, J. M.; Joshi, N.; Hartman, R. L. "Interfacial properties of asphaltenes at the Heptol-Brine interface." *Energy & Fuels,* **2015,** 30 (1), 80 – 87.

(17) Farooq, U.; Simon, S.; Tweheyo, M. T.; Øye, G.; Sjöblom, J.; "Interfacial tension measurements between oil fractions of a crude oil and aqueous solutions with different ionic composition and pH." *Journal of Dispersion Science and Technology,* **2013**, 34 (5), 701 – 708.

(18) Rane, J. P.; Harbottle, D.; Pauchard, V.; Couzis, A.; Banerjee, S.; "Adsorption kinetics of asphaltenes at oil-water interface and nanoaggregation in the bulk." *Langmuir,* **2012**, 28 (26), 9986 – 9995.

(19) Bouriat, P.; Kerri, N. E.; Graciaa, A.; Lachaise, J.; "Properties of a two-dimensional asphaltene network at the water-cyclohexane interface deduced from dynamic tensiometry." *Langmuir,* **2004**, 20 (18), 7459 – 7464.

(20) Pauchard, V.; Rane, J. P.; Zarkar, S.; Couzis, A.; Banerjee, S.; "Long-term adsorption kinetics of asphaltenes at the oil-water interface: a random sequential adsorption perspective." *Langmuir,* **2014**, 30 (28), 8381 – 8390.

(21) Jennings, H. Y. JR.; "The effect of temperature and pressure on the interfacial tension of benzene-water and normal decane-water." *Journal of collid and interface science,* **1967,** 24, 323 – 329.

(22) Hu, C.; Garcia, N. C.; Xu, R.; Cao, T.; Yen, A.; Garner, S. A.; Macias, J. M.; Joshi, N.; Hartman, R. L., Interfacial Properties of Asphaltenes at the Heptol–Brine Interface. *Energy & Fuels* **2016,** *30*, 80-87.

(23) Czarnecki, J.; Moran, K., On the stabilization mechanism of water-in-oil emulsions in petroleum systems. *Energy & Fuels* **2005,** *19*, 2074-2079.

(24) He, Kai, Christina Nguyen, Ramya Kothamasu, Liang Xu, and others. "Insights into Whether Low Salinity Brine Enhances Oil Production in Liquids-Rich Shale Formations." *EUROPEC 2015*. Society of Petroleum Engineers, 2015.

(25) Silva Ramos, Antônio Carlos da, Lilian Haraguchi, Fábio R. Notrispe, Watson Loh, and Rahoma S. Mohamed. "Interfacial and Colloidal Behavior of Asphaltenes Obtained from Brazilian Crude Oils." *Journal of Petroleum Science and Engineering* 32, no. 2 (2001): 201–216.

(26) Bos, Martin A., and Ton van Vliet. “Interfacial Rheological Properties of Adsorbed Protein Layers and Surfactants: A Review.” *Advances in Colloid and Interface Science* 91, no. 3 (2001): 437–471.

(27) Nguyen, D.; Balsamo, V.; Phan, J., Effect of Diluents and Asphaltenes on Interfacial Properties and Steam-Assisted Gravity Drainage Emulsion Stability: Interfacial Rheology and Wettability. *Energy & Fuels* **2014,** *28*, 1641-1651.

(28) Aske, Narve, Robert Orr, Johan Sjöblom, Harald Kallevik, and Gisle Øye. “Interfacial Properties of Water–crude Oil Systems Using the Oscillating Pendant Drop Correlations to Asphaltene Solubility by near Infrared Spectroscopy.” *Journal of Dispersion Science and Technology* 25, no. 3 (2004): 263–275.

(29) Zarkar, Sharli, Vincent Pauchard, Umer Farooq, Alexander Couzis, and Sanjoy Banerjee. “Interfacial Properties of Asphaltenes at Toluene–water Interfaces.” *Langmuir* 31, no. 17 (2015): 4878–4886.

(30) Alves, Douglas R., Juliana SA Carneiro, Iago F. Oliveira, Francisco Façanha, Alexandre F. Santos, Claudio Dariva, Elton Franceschi, and Montserrat Fortuny. “Influence of the Salinity on the Interfacial Properties of a Brazilian Crude Oil–brine Systems.” *Fuel* 118 (2014): 21–26.

Chapter 2 Experimental Techniques

2.1 Contact Angle Goniometer and Tensiometer

The standard goniometer used is ramé-hart Model 250 F4 series specially hand crafted for University of Alberta by ramé-hart instrument co. This standard goniometer mainly consists of light illuminator, camera, microsyringe and leveling stage for either contact angle or surface tension measurement.

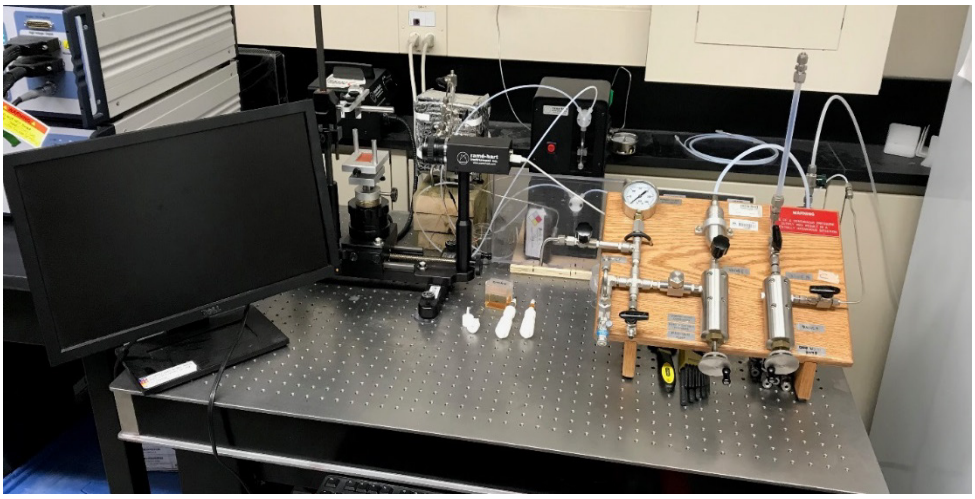

Figure 2. 1 Contact angle goniometer and tensiometer built by Ramé-hart Instrument Company

Since the experiment is conducted under elevated temperature and pressure, a heating chamber has been specially made for this application. The chamber is constructed with aircraft grade aluminum with two circular sighting windows in line. The syringe penetrated through the top of the chamber and can be illuminated and observed by optical camera. The heating chamber is rated for 230 °C and 1000 psi. On the back side of the heating chamber, a cartridge style heating element with 400 W of power bolted on the exterior of the chamber. On the front side of the chamber, a variety of NPT threads are fitted with temperature sensor, pressure control/relief, sample in and sample out.

A temperature controller measured the chamber temperature and maintain at desired test temperature.

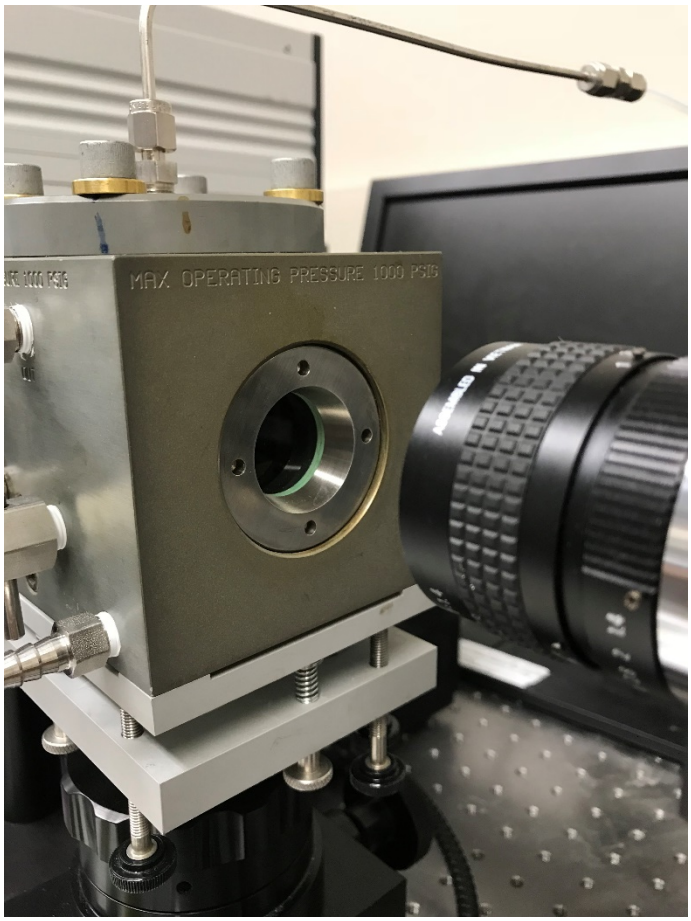

Figure 2. 2 Heating Chamber with sighting windows and optical camera

Two hand-cranked pumps are used to introduce the bulk liquid and drop phase into the chamber. The bulk liquid was firstly delivered into the chamber by pressure differential. Then, hand cranked pump was used to consistently apply the pressure to the vessel. A backflow regulator was used to control the maximum pressure of the chamber. Any excess liquid pressure can be released through exit tube. For the drop phase pump, after initial flushing of the tubing, the drop size can be controlled by carefully dialling the pump. Finally, operators can adjust the size of drop phase to a desired level.

For this study, the maximum temperature reached in the testing was 120 ºC due to the wattage of heating element. The maximum pressure reached in the testing is 413 kPa to maintain the water and solvent in liquid state. Additionally, a dispenser and an oscillator were purchased to study dilatational interfacial properties. The dispenser and oscillator differ in volume and speed. The oscillator delivered tiny amount of volume less than 10 uL but can oscillator fast up to 5 Hz with sinusoidal wave form.

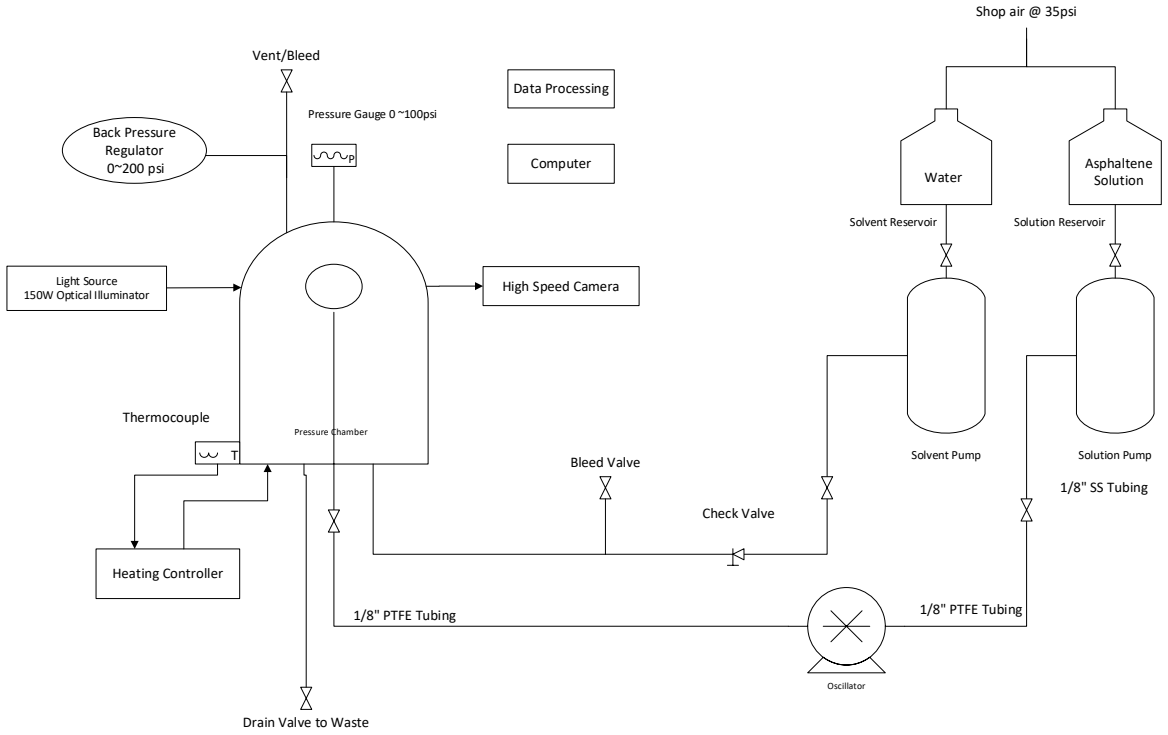

Figure 2. 3 Schematic Diagram of High Temperature High Pressure Oscillating Drop Goniometer

For this study, dilatational interfacial properties at high temperature and high pressure was investigated. Tremendous amount of effort was spent to modify and pressure-proof the instrument to perform high pressure oscillation. A series of parts have been replaced with premium quality stainless steel valves and gauges. Since the pressure is not over 413 kPa at 120 ºC, PFA flexible

tubing was used for any transfer line for visualization and low residue due to smooth inner wall finish.

The bulk phase (aqueous phase most of the case) was first introduced into the pressure chamber by applying air pressure to force the liquid flow through. At the top of the chamber, a sample exit valve was used to purge any residue air present in the system. After the chamber had been flushed with the desired bulk phase, the pressure in the chamber is equal to air pressure in the solvent reservoir. If additional pressure is required, the solvent pump can be filled with bulk phase, by changing the opening and closing action of two valves, the bulk phase can be introduced into the pump and then reached desired pressure. To maintain the pressure, back pressure regulator is connected to the pressure chamber, any excess pressure caused by any pumps, oscillator or heat expansion can be discharged as liquid into the waste beaker.

After the bulk phase had been introduce into the pressure chamber, hand crank pump can be used to introduce drop phase into the pressure chamber. By carefully cranking the drop phase pump and flush the sample line, one can adjust the pendant drop to desired size for experiment. Operator can either choose to use interfacial measurement or connect to an oscillator for dilatational property measurement.

2.2 Pendant drop shape method

Interfacial and surface tension of liquids are crucial to many processes in the chemical and petroleum industry. There is a need for a fast and easy technique with satisfactory accuracy and reproducibility. Traditionally, Du Noüy ring and Wilhelmy plate methods are utilized throughout the industries and research laboratories. These types of techniques are well suited for surface tension and IFT measurement but also time consuming. Drop shape analysis has usually been performed by photographing a droplet in an optical path environment, and then the characteristic sizes of the droplet can be measured on the photographic prints. Since the advancement of digital photography technology and computer processing ability, the droplet sizes can be recorded instantly by a charged-coupled device (CCD) camera and processed in real time with minimal latency. The obtained sizes and shapes were then further fitted to Laplace equation to calculate IFT.

Figure 2.3 shows a cross-sectional view of a pendant drop. Due to the symmetrical shape of the pendant drop, it is convenient to designate the z the axial coordinate and x the radial coordinate. The origin is set at the apex of the drop. The arc length coordinate, s, which is the distance of the drop contour from the apex. The x-z coordinates of the droplet profile can be expressed as functions of the parameter s. The angle that the surface tangent makes with the x-axis is φ, which is also the angle of the surface normal with respect to the z-axis.

The Young-Laplace equation states that the pressure drop across a curved interface is

$$\Delta P = \Delta P_{internal} - \Delta P_{external} = \sigma \left\{ \frac{1}{R_1} + \frac{1}{R_2} \right\} \tag{2.1}$$

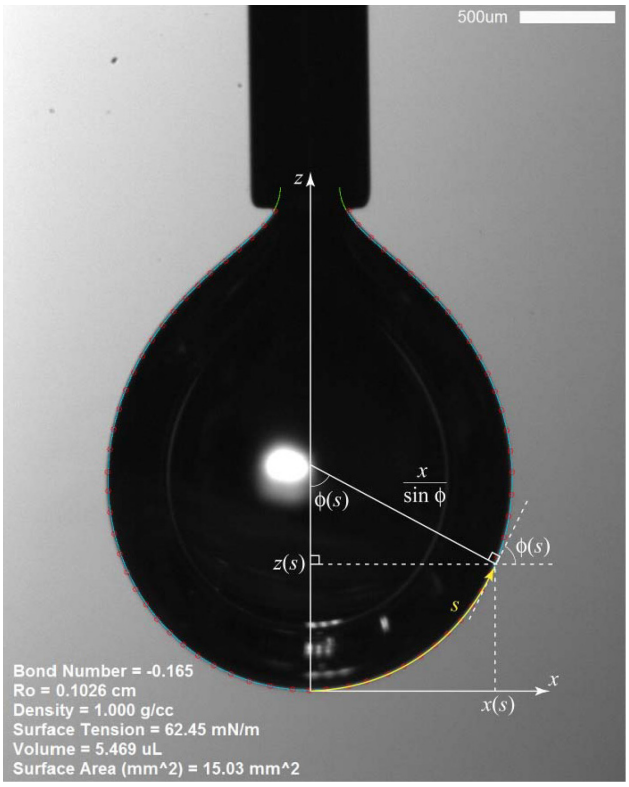

Figure 2. 4 A pendant drop image showing the coordinate system used for determining the surface tension. [1]

Where R_1 and R_2 are the principal radii of curvature. For the convenience, R_1 is set to be the principal curvature in the *x*-*z* plane and the R_2 is set to be the principal curvature perpendicular to the *x*-*z* plane.

At the apex (s=0), both radii of curvature are equal to a value designate as R_0.

$$\Delta P\ (s = 0) = \frac{2\sigma}{R_0} \tag{2.2}$$

At higher position from the apex, additional hydrostatic force due to gravitational effects from the difference in densities

$$\Delta P(s) = \frac{2\sigma}{R_0} + g\Delta\rho z(s) \tag{2.3}$$

Where $\Delta\rho = \rho_{external} - \rho_{internal}$. Combining Equation 2.1 and 2.3 for the pressure drop are equivalent:

$$\Delta P(s) = \frac{2\sigma}{R_0} + g\Delta\rho z(s) = \sigma\left(\frac{1}{R_1} + \frac{1}{R_2}\right) \tag{2.4}$$

Substituting $\frac{1}{R_1} = \frac{d\varphi}{ds}$ and $\frac{1}{R_2} = \frac{sin\varphi}{x}$ into Equation 2.4

$$\frac{2\sigma}{R_0} + g\Delta\rho z(s) = \sigma\left(\frac{d\varphi}{ds} + \frac{sin\varphi}{x(s)}\right) \tag{2.5}$$

And solving for $\frac{d\varphi}{ds}$ yields

$$\frac{d\varphi}{ds} = \frac{2}{R_0} + \frac{g\Delta\rho}{\sigma} z(s) - \frac{sin\varphi}{x(s)} \tag{2.6}$$

From the geometry, the terms can be written as

$$\frac{dx}{ds} = cos\varphi \tag{2.7}$$

$$\frac{dz}{ds} = sin\varphi \tag{2.8}$$

Combining Equation 2.6 – 2.8 making a first order system of non-linear differential equations, with initial condition $x(0) = z(0) = \varphi(0) = 0$, the equilibrium drop profile can be obtained. It is convenient to choose R_0 as a characteristic length scale. If $\bar{x} = x/R_0$, $\bar{z} = z/R_0$, and $\bar{s} = s/R_0$. Equation 2.6 – 2.8 become

$$\frac{d\varphi}{d\bar{s}} = 2 + N_{Bd}\bar{z}(\bar{s}) - \frac{sin\varphi}{\bar{x}(s)} \tag{2.9}$$

$$\frac{d\bar{x}}{d\bar{s}} = cos\varphi \tag{2.10}$$

$$\frac{d\bar{z}}{d\bar{s}} = sin\varphi \tag{2.11}$$

Where a dimensionless Bond number is defined as

$$N_{Bd} = \frac{g\Delta\rho R_0^2}{\sigma} \tag{2.12}$$

Integrating Equation 2.9 -2.11 with the rescaled initial conditions, $\bar{x}(0) = \bar{z}(0) = \varphi(0) = 0$, a series of curves only relating a function of N_{Bd} can be generated. Drop profiles are fit using an optimization routine (Rotenberg) that determines the location of apex (offsets for the *x* and *z* coordinates), scaling factor (R_0), and shape (N_{Bd}). With these optimized values of R_0 and N_{Bd} and knowledge of density difference and gravity, the surface tension can be calculated from Equation 2.12 as:

$$\sigma = \frac{g\Delta\rho R_0^2}{N_{Bd}} \tag{2.13}$$

Reference

(1) Lisa Mondy, Carlton Brooks, Anne Grillet, Harry Moffat, Tim Koehler, Melissa Yaklin, Matt Reichert, Lynn Walker, Raymond Cote, Jaime Castañeda, Surface Rheology and Interface Stability, SAND2010-7501 Unlimited Release Printed November 2010.

Chapter 3. Adsorption Kinetics of Asphaltenes at Oil/Water Interface: Effects of Temperature, Addition of Surfactant and Aromaticity of Solvent

3.1 Introduction

Asphaltenes are one of most complicated portions of hydrocarbons in the crude oil in petroleum industry and majority of research done on crude oil have focused on asphaltenes. Asphaltenes are defined conventionally as a solubility class that is soluble in aromatic solvent such as toluene or xylene but insoluble in aliphatic solvent such as pentane or hexane [1]. Asphaltenes are the heaviest with typical molecular weight in the range of 400 Da to 1000 Da and polar components consisting of aromatic hydrocarbon rings with peripheral aliphatic chains, containing heteroatoms such as nitrogen, oxygen and sulphur as well as metal elements such as vanadium, nickel and iron [2,3].

In the Athabasca region where heavy oil and bitumen are dominant in the Northern Alberta. Asphaltene contents are usually higher compared to rest of the world. In the mining industry, the formation of water-in-oil emulsion is unavoidable and cause processability issues such as high water and salt content in the crude oil products. These high water and salt content cause contribution to corrosion issues for downstream upgraders. In Steam-assisted Gravity Drainage (SAGD) system, more complicated oil-in-water emulsions recovered from the ground and then processed by surface facility results in water-in-oil emulsions. The water containing crude oil have negative impact on the economics of these oil producers. Asphaltenes are believed to play a crucial role of stabilizing such water-in-oil and oil-in-water emulsion system. In addition, the presence o resins [4] and solid fines and clays from various minerals [5] with addition of asphaltenes adsorbed

to the oil/water interface which is often considered as irreversible process can significantly stabilize the complex oil-in-water emulsions. With elongated processing time, asphaltenes present in the oil/water interface often form rigid film [6-8] which prevent liquid phase coalescence which results in unresolved emulsion [9].

The effect of temperature and pressure on the interfacial tension for pure solvent system has been studied long time ago. The effect of the pressure on interfacial tension for various solvents was minimal compared to that of temperature [10]. With less than 200 atmospheric pressure, there is no significant change in IFT. However, with temperature increase from 25 °C to 100 °C, significant decrease of IFT was observed. With the maximum SAGD surface processing facility operating pressure less than 15 atmospheric pressure, the effect of pressure will be ignored for this study.

With increasing aging time, more asphaltene molecules adsorb to the oil/water interface which leads to gradual decrease of IFT. Compared to surfactants, asphaltenes has larger molecular weight and is less surface active, it is much more difficult for asphaltenes to reach a steady state. The time reaching to the equilibrium could be a few hours [11]. From the studies of aging time, the adsorption process for asphaltenes is a slow process compared to surfactant reconfiguration. The equilibrium IFT for asphaltenes was empirically obtained.

The diluent used to reduce the density and viscosity of the bitumen come from different sources and their composition varies greatly. As the ratio of aromatic to aliphatic components varies, the aromaticity of the organic phase is important. One study found that as the volume percentage of the aliphatic solvent increases, the IFT shows increasing trend gradually [22]. However, for this set of experiment, the results shown as the composition of aliphatic solvent increases, the IFT decreases even though the samples are different. Asphaltenes dissolved in “good solvent” like

toluene will reach equilibrium faster than “poor solvent” such as pentane and heptane at higher concentrations. Except the adsorption time, the effect of the solvent also correlates to the emulsion stability. The emulsion stability has been reported that with the increasing heptane volume percentage, the stability increases at first and reached a peak, and finally decreases. For this study, the solvent effect of toluene versus heptane combination was investigated.

In Athabasca oil, it is generally believed that the bitumen surrounded by hydrophilic water films and then the bitumen can be extracted by aqueous solution [13]. However, in this watery layer, it also contains salt accumulated from the formation. During the extraction process, the emulsified water contains salt is present in the oil phase. It is crucial to investigate the impact of monovalent salt (mostly in form of chloride salt) to the IFT between oil and water interface. With increasing concentration of potassium chloride, the IFT of crude oil system was found to decrease slightly within a low salinity range and increase afterwards. It was proved that the existence of potassium chloride would affect the oil recovery [14].

It is important to study the adsorption kinetics of asphaltenes at the oil/water interface at elevated temperature since at SAGD field, about 200 °C of steam was used to extract bitumen from underground. Once reached to the surface facility, the temperature is lowered to 120 ~ 130 °C. One study found that there was no significant influence on adsorption in the range of 5 °C to 45 °C for asphaltenes extracted from Brazilian crude oils [15]. Other study shows that IFT and elastic moduli at oil/water interface shown little relevance with temperature varying from 23 °C to 60 °C. In this study, even higher temperature was used to study adsorption kinetics of asphaltenes at different temperatures.

3.2 Materials and Methods

3.2.1 Materials

In this study, Milli-Q water (resistance of ≥18.2 MΩ·cm) was used to prepare all aqueous solutions. ACS grade of Toluene and n-heptane were purchased from Fisher Scientific Canada.

The chemical used for this study is Pluronic® L-64 block copolymer surfactant from BASF. The composition of the polymer is poly (ethylene glycol)-block-poly (propylene glycol)-block-poly (ethylene glycol) and is short for PEG-PPG-PEG. This polymer has average molecular weight of 2900 Da. CAS number is 9003-11-6. The chemical was purchased through Sigma Aldrich.

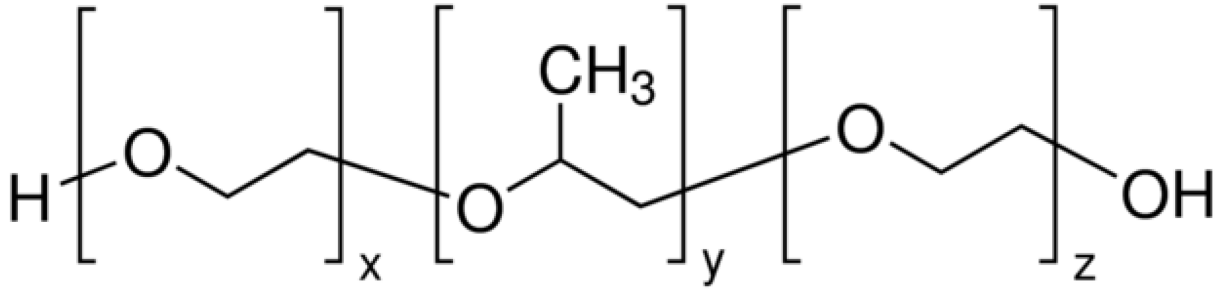

Figure 3. 1 Chemical Structure of PEG-PPG-PEG Pluronic® L-64 block copolymer surfactant.

3.2.2 Asphaltene sample preparation

Bitumen sample was obtained from a SAGD facility. The sample was first purified by Dean Stark Extraction process according to ASTM D6560 procedure [16] using toluene reflux. Then the purified bitumen toluene solution was concentrated, toluene was removed from the bitumen in the oven. The purified bitumen was then thoroughly mixed with n-heptane with 1:1 ratio and finally diluted to 40:1 n-heptane to bitumen ratio (wt:wt) in order to precipitate maximum amount of asphaltenes. Asphaltenes particles were filtrated and washed with n-heptane to remove any

bitumen residue until the solvent is colorless. Finally, the asphaltene sample were dried, ground into powder and store in desiccator before use.

The asphaltene was measured to exact mass and dissolved in toluene, 7:3 v/v toluene/n-heptane and 1:1 v/v toluene/n-heptane to make up 1 % stock solution. Further dilution is required for targeting 1000 ppm solution. The asphaltenes solution is preserved in closed container at 4 ºC to minimize oxidation and evaporation. Before each experiment, the desired asphaltene solution was sonicated for 5 minutes and degassed for additional 5 minutes to eliminate any possible bubbles present in the solution.

The PEG-PPG-PEG polymer is in viscous liquid form. Exact weight amount of 1.0000 gram of polymer was placed in the volumetric flask, shook well and finally diluted to 1000 mL as 0.1 % (1000 ppm) stock solution. For testing, final dilution to 100 ppm and 25 ppm was utilized.

3.3 Results and Discussion

3.3.1 Effect of Asphaltenes Concentrations: Dynamic interfacial tension versus time

The effect of asphaltenes concentrations from 50 to 2000 ppm was first studied to establish the experimental baseline.

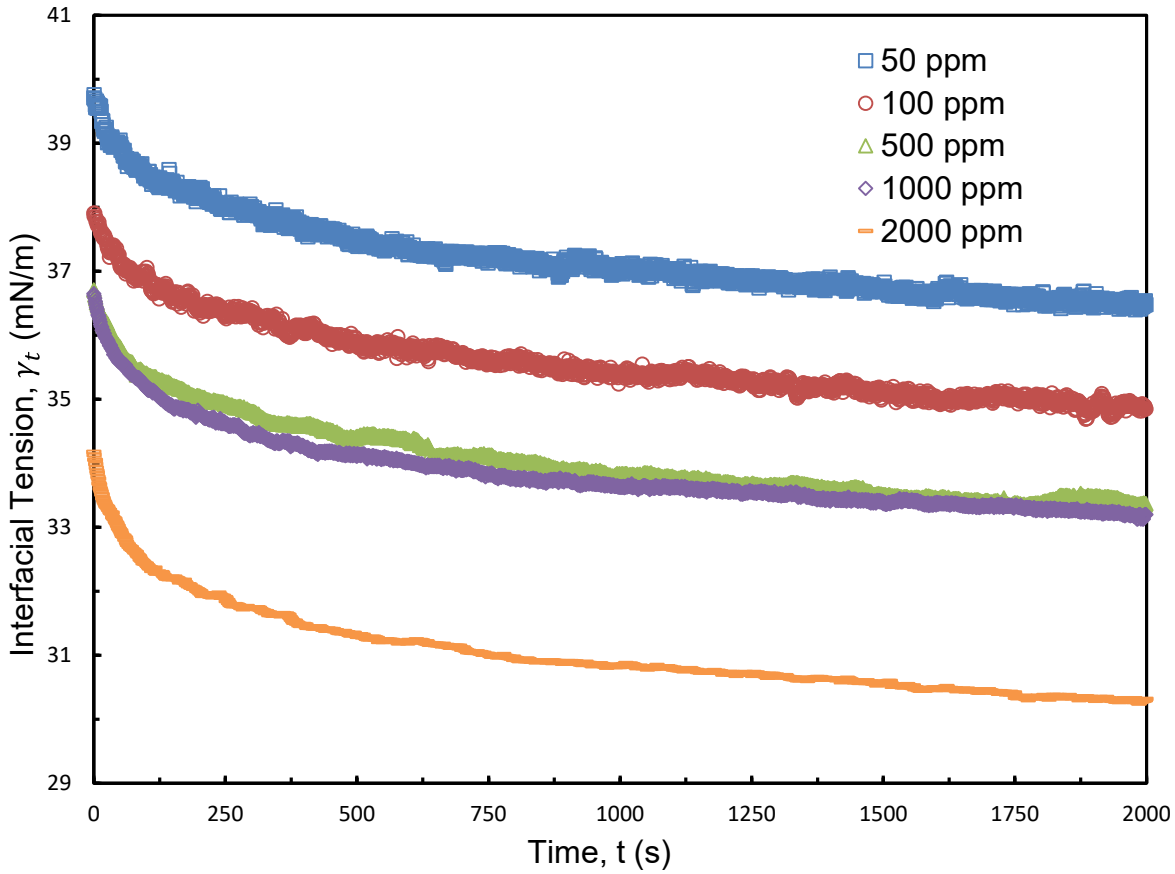

Figure 3. 2 Dynamic IFT of Concentration of 50, 100, 500, 1000 and 2000 ppm of asphaltene in toluene pendant drop in water system vs. time at 23 ºC.

A general trend can be observed for the dynamic IFT curves in Figure 3.2: (1) initially, the IFT decreases exponentially within seconds; (2) the reduction starts to flatten out; (3) the reduction seems to be infinite, even after 5000 seconds of time elapsed, which indicates the system still did not reach to equilibrium. Initially for the first 250 seconds, the rapid reduction of interfacial tension

is defined by a diffusion controlled process. The asphaltenes adsorbed at oil and water interface is resemble to large molecular weight of proteins at air and water interface [17]. For diffusion controlled process, Ward-Tordai equation is generally used to describe such behavior as in Equation 3.1.

$$\Gamma_t = 2\sqrt{\frac{D}{\pi}} C_0 \sqrt{t} \tag{3.1}$$

Where Γ_t is the surface excess concentration of materials in this case it is asphaltenes on the interface at time t. D is the diffusion coefficient of asphaltenes moving to the interface. C_0 is the bulk concentration of asphaltenes. According to Sheu [18], the surface excess concentration Γ_t can be correlated to the surface pressure by Equation 3.2 where γ_0 and γ_t are the interfacial tension at time zero t=0 and arbitrary time t. R is the gas constant with the value of 8.314 J/(mol·K), and T is the temperature,

$$\Pi = \gamma_0 - \gamma_t = \Gamma_t RT \tag{3.2}$$

Combining Equations 3.1 and 3.2, the Gibbs-Duhem diffusion equation can be deduced as shown in Equation 3.3,

$$\gamma_t = \gamma_0 - 2RT\sqrt{\frac{D}{\pi}} C_0 \sqrt{t} \tag{3.3}$$

According to Equation 3.3, γ_t should be proportional to $\sqrt{t}$ initially for a diffusion-controlled process. Therefore, Figure 3.2 was replotted as IFT vs. $\sqrt{t}$ as shown in Figure 3.3.

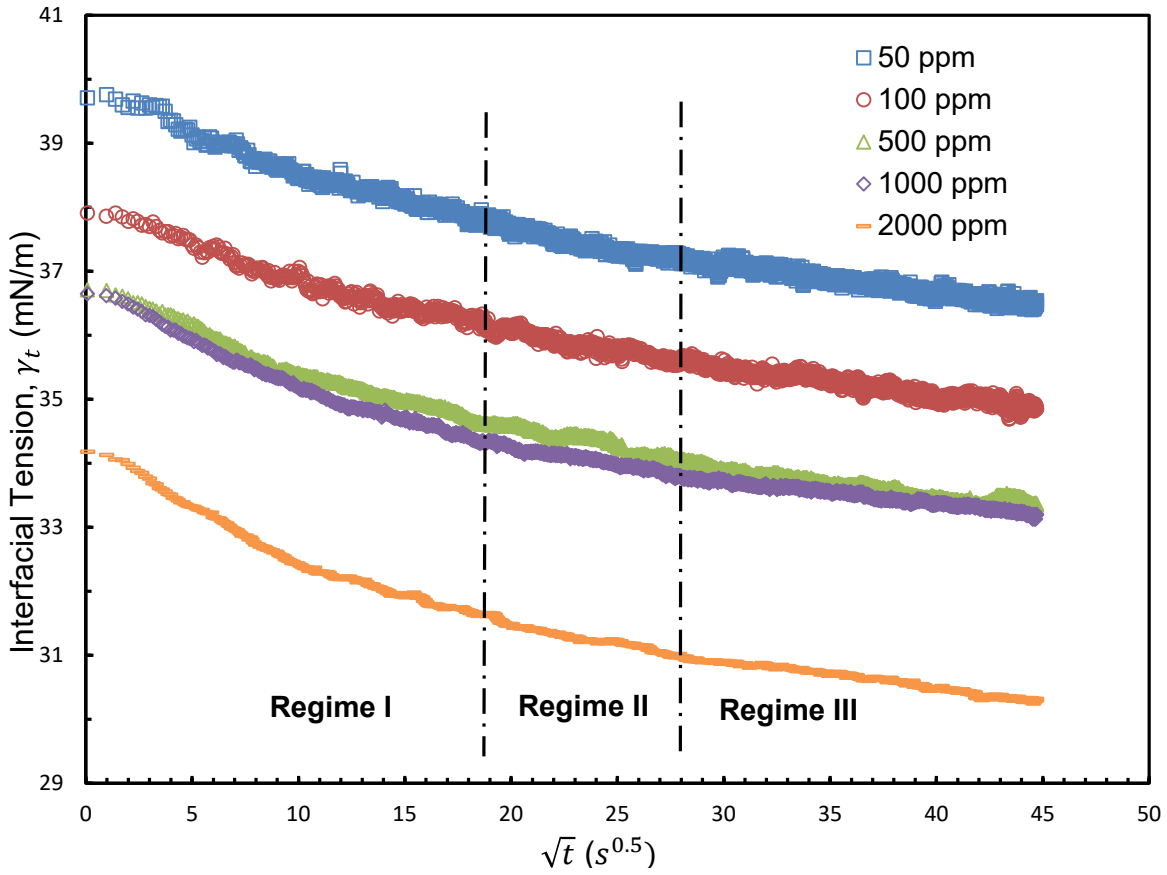

Figure 3. 3 Dynamic IFT vs. $\sqrt{t}$ for 50, 100, 500, 1000 and 2000 ppm asphaltenes in toluene pendant drop in water system at 23 °C.

Five curves at different asphaltenes concentrations in the Figure 3.3 can be fitted with 2nd order polynomial trend line with R square value of 0.99 and above. It indicates that the curves consist of three portions of relatively straight linear relationships. These three portions of regions are divided into Regime I, II and III with dash lines in Figure 3. Regime I demonstrates the rapid reduction of IFT along with time when a fresh drop of asphaltenes in toluene exposed to the water phase. Regime III is the stage where the adsorption process reaches to equilibrium slowly. Regime II is the transition stage between Regime I and Regime II.

Regime I. During the initial stage of asphaltenes adsorption, all five curves in Figure 3.3 shows a linear correlation between IFT and √T. The Ward-Tordai model (3.1) and the Gibbs-Duhem diffusion model (3.3) can be used to fit the curves. Such behavior is similar to the adsorption of proteins onto air-liquid interface or liquid-liquid interface [17, 19-22]. In Regime I, the asphaltene behavior at toluene/water interface was dominated by diffusion controlled process. As the concentration increases, subtle steeper slopes were observed.

Table 3. 1 Respective slopes and diffusion coefficients for Regime I for 50, 100, 500, 1000 and 2000 ppm of asphaltenes in water at 23 °C

	50 ppm asphaltenes solution at 23 °C	100 ppm asphaltenes solution at 23 °C	500 ppm asphaltenes solution at 23 °C	1000 ppm asphaltenes solution at 23 °C	2000 ppm asphaltenes solution at 23 °C
Slopes	-0.099	-0.090	-0.103	-0.113	-0.121
Diffusion Coefficient, D (m^2/s)	$5.08x10^{-13}$	$1.05x10^{-13}$	$5.50x10^{-15}$	$1.65x10^{-15}$	$4.76x10^{-16}$

Based on Figure 3.3 and Table 3.1, the slopes and γ_0 can be directly obtained from the linear regression of IFT data in Regime I. The diffusion coefficient D is the absolute value of the slope k in Regime I of Figure 3.3. Described in Equation 3.4.

$$D = \pi \left(\frac{k}{2RTC_0}\right)^2 \tag{3.4}$$

As observed in Table 3.1, the diffusion coefficient of asphaltenes to toluene/water interface decreases as the concentration of the asphaltenes solution increases from 50 ppm to 2000 ppm.

Regime II. Regime II is a transition regime between the Regime I and Regime III. In Figure 3.3 where Dynamic IFT vs. √t, a non-linear relationship was shown. As the time progress from 500 to 1000 seconds, a slowdown of reduction in IFT was observed. The possible explanation is that as the population of asphaltenes at oil/water interface increases, the adsorption is impeded by steric hindrance due to the size of the asphaltenes molecules. The results are consistent with the previous studies which suggest that after reaching 35 ~ 40 % of asphaltene coverage, the adsorption rate of asphaltenes could decline [23].

Regime III. In Regime III, the dynamic IFT continues to decrease but with reduced rate compared to Regime I and II. At this stage, the toluene/water interface has already been pre-occupied by previously adsorbed asphaltenes. Asphaltenes continue to migrate to the interface because of the nature of their properties. The resulted long term reduction of IFT could be explained by reconfiguration of adsorbed asphaltenes at the interface with long relaxation time [17, 21, 24]. The Ward-Tordai equation successfully illustrates the diffusion-controlled process in Regime I but does not explain the behavior of long-term adsorption. A correlation reported by Yarranton shows that the equilibrium IFT can be described with long term adsorption [25]. It shows that the dynamic IFT at long term is proportional to the inverse square root of time (1/√t):

$$\gamma(t)_{t\to\infty} = \gamma_{eq} + \frac{RT\Gamma^2}{C_0}\sqrt{\frac{7\pi}{12Dt}} \tag{3.5}$$

Where C_0 is the asphaltenes concentration (mol/m^3), γ_{eq} is the interfacial tension at equilibrium state, Γ is the surface excess concentration at saturation and D is the diffusion coefficient in Regime III.

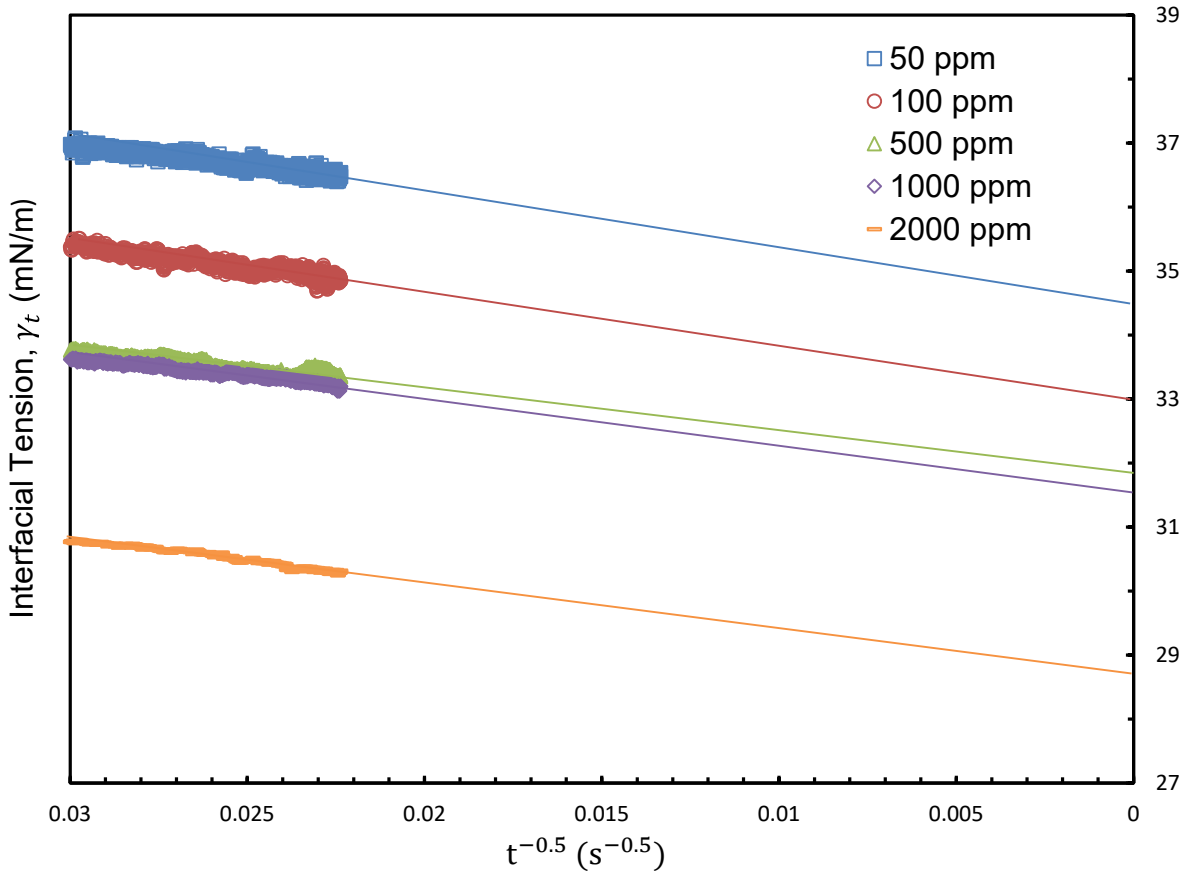

Figure 3. 4 Plots of γ_t vs. $t^{-0.5}$ for 50, 100, 500, 1000 and 2000 ppm of asphaltenes pendant drop in water at 23 °C (the x-axis is in reverse order)

Figure 3.4 shows that the extrapolating γ_t vs. $t^{-0.5}$ by linear regression to obtain γ_{eq}. The equilibrium values shown on the intercepts on Y axis on the right side. The Figure 3.4 shows that as the concentration of asphaltenes solution increases, the final equilibrium dynamic IFT decreases gradually.

3.3.2 Effect of System Temperature

For effect of system temperature on dynamic IFT of asphaltenes/water interface, 1000 ppm of concentration was selected to perform all temperature study.

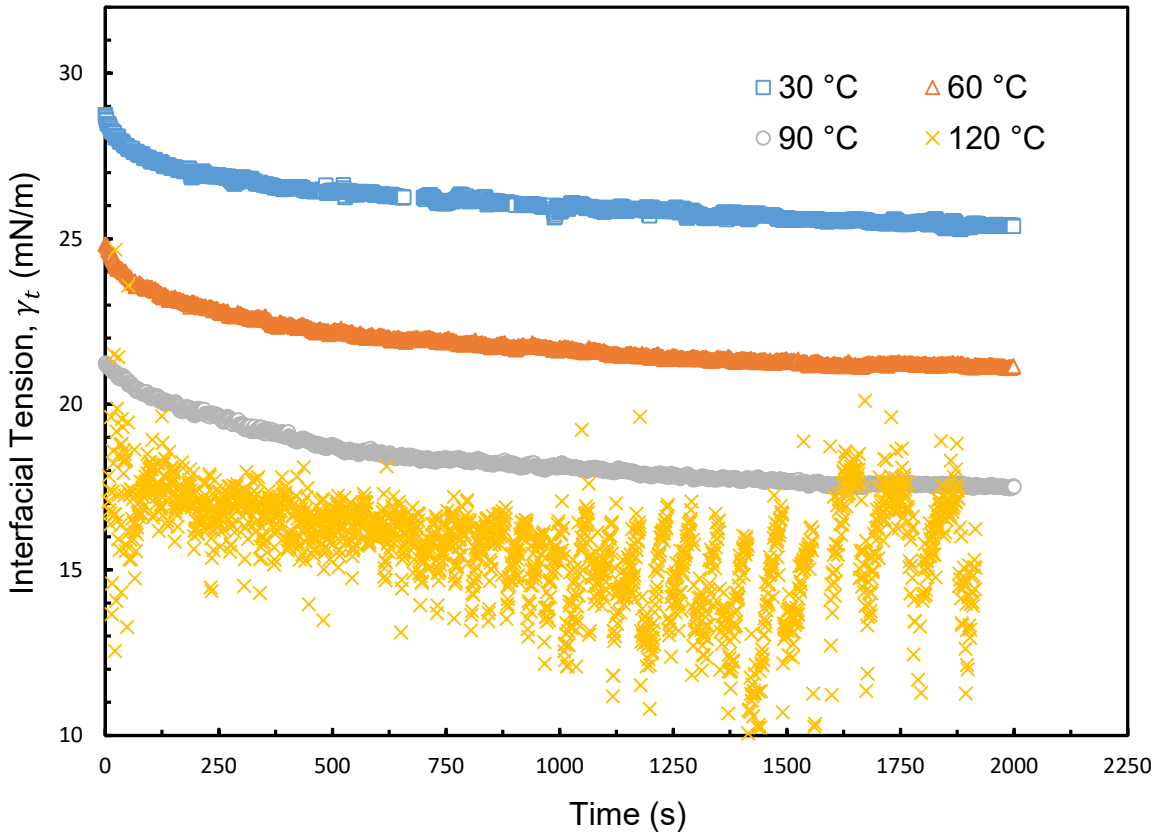

Figure 3. 5 Dynamic IFT of 1000 ppm of asphaltene in toluene pendant drop in water system vs. time at 30, 60, 90 and 120 ºC.

Figure 3.5 shows the dynamic IFT between 1000 ppm asphaltene toluene solution pendant drop suspended in deionized water at 30, 60, 90 and 120 ºC. As shown in Figure 3.5, at 30 ºC, the dynamic IFT decreases exponentially with first few hundred seconds and then the gradual

reduction of IFT slows down with time. For all the temperature ranges from 30 to 90 ºC, the same trend has been observed. However, the difference between 60 and 90 ºC IFT curve seems to be less than that between 30 and 60 ºC. At 120 °C, the dynamic IFT fluctuates with much larger magnitude. There are several explanations to this phenomenon: first, due to the position of the heating elements located at the bottom of the vessel, during heating, convection current circulates inside the pressure chamber causing the drop to become slightly distorted hence more fluctuating reading. Secondly, the heating program is based on a feedback loop, frequent heating and heat loss (due to heat shutoff) causing the expansion and contraction of the drop phase liquid (asphaltenes solutions). Possible improvements are suggested in Chapter 5. However, the general trend is still observed: as the temperature increases from 30 to 120 °C, the dynamic IFT decreases significantly. Between 90 to 120 °C, the IFT reduction is not pronounced as from 30 to 60 °C or 60 to 90 °C.

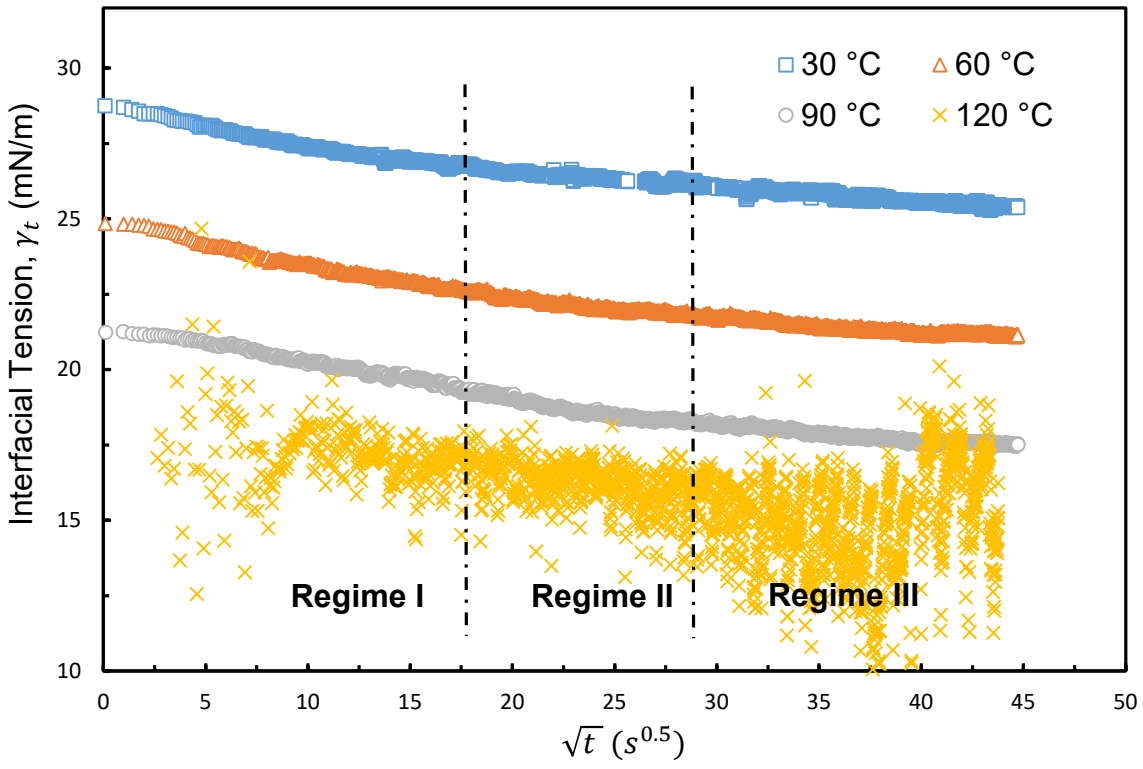

Figure 3. 6 Dynamic IFT vs. $\sqrt{t}$ for 1000 ppm asphaltenes in toluene pendant drop in water system at 30, 60, 90 and 120 °C.

Regime I: Similar approach is applied as in Chapter 3.3.1. The Figure 3.6 plots IFT vs $\sqrt{t}$ of 1000 ppm asphaltenes in toluene pendant drop in water at 30, 60, 90 and 120 °C. After the root square of time conversion in the X axis, the curves can be divided into three regimes similar in Chapter 3.3.1. For 120 °C curve, the slope value was optimized and approximate due to large fluctuation of the data. For Regime I, their respective slopes and diffusion coefficients were calculated and tableted in Table 3.2.

Table 3. 2 Respective slopes and diffusion coefficients for Regime I for 1000 ppm of asphaltenes in water at 30, 60, 90 and 120 °C

	1000 ppm asphaltenes toluene pendant drop in water solution at 30 °C	1000 ppm asphaltenes toluene pendant drop in water solution at 60 °C	1000 ppm asphaltenes toluene pendant drop in water solution at 90 °C	1000 ppm asphaltenes toluene pendant drop in water solution at 120 °C
Slopes	-0.113	-0.132	-0.120	-0.2 (approximate)
Diffusion Coefficient, D (m^2/s)	$1.58x10^{-15}$	$1.78x10^{-15}$	$1.24x10^{-15}$	$2.94x10^{-15}$ (approximate)

From Table 3.2, for 1000 ppm asphaltenes in toluene/water system, as the system temperature increases from 30 to 120 °C, the slope decreases gradually and accelerated dynamic IFT reduction

was observed. As the temperature increases, the diffusion coefficient increases as well. From 30 to 120 °C, the diffusion coefficient double in value from 1.58 x 10^{-15} to 2.94 x 10^{-15} m^2/s.

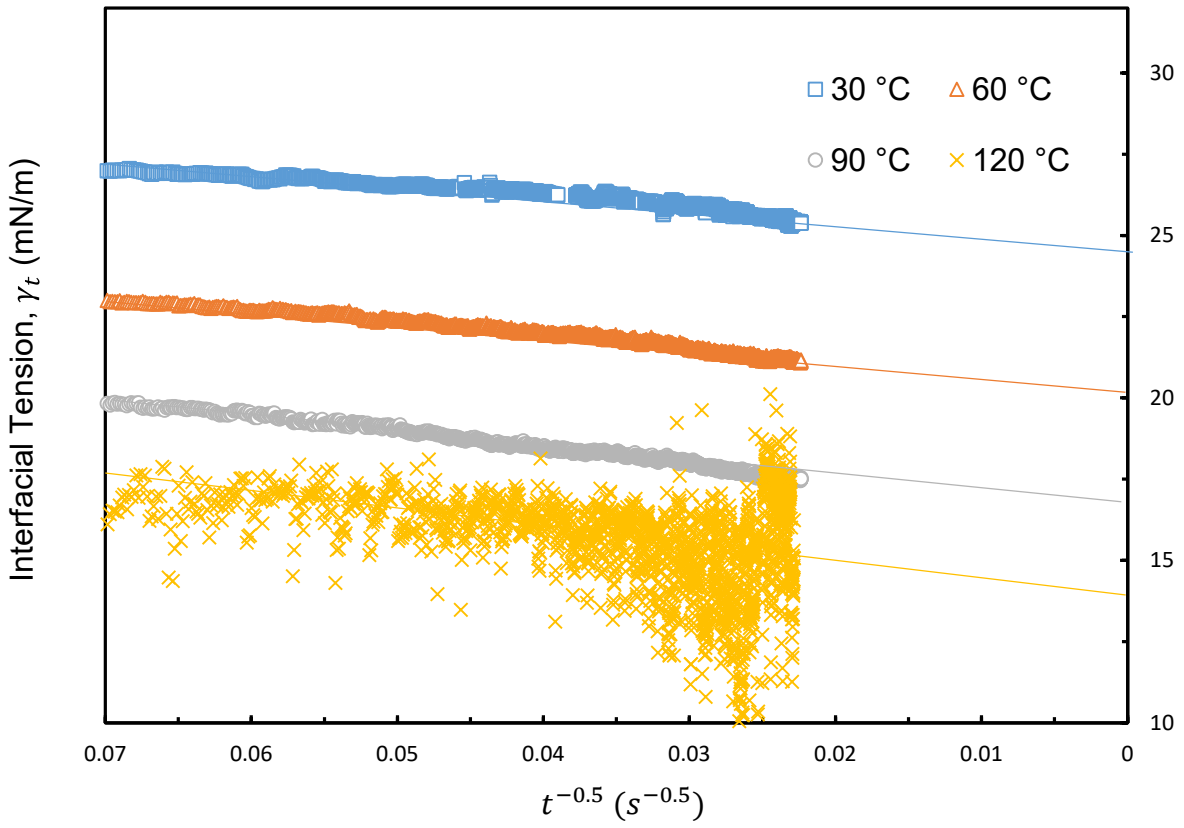

Figure 3. 7 Plots of γ_t vs. $t^{-0.5}$ for 1000 ppm asphaltenes pendant drop in water at 30, 60, 90 and 120 °C (the x-axis is in reverse order)

Regime III: Figure 3.7 shows that the extrapolating γ_t vs. $t^{-0.5}$ by linear regression to obtain γ_{eq}. The equilibrium values shown on the intercepts on Y axis on the right side. The Figure 3.7 shows that as the temperature increases, the final equilibrium dynamic IFT decreases proportionally. The reduction of equilibrium IFT at from 90 to 120 °C was not pronounced as the those from 60 to

90 °C and 30 to 60 °C. Therefore, at lower temperatures, increasing temperature has largest return in decreasing IFT.

3.3.3 Effect of Addition of PEG-PPG Polymer for Asphaltenes Adsorption Process

For this Chapter, a PEG-PPG polymer Pluronic L-64 is added into the bulk phase. Based on preliminary testing, the dosage selected for L-64 is 25 ppm in bulk water phase. At elevated dosage of L-64, the bulk phase became turbid and the IFT measurement was not possible with optical approach. At elevated temperature of 120 °C, the optical approach is also not possible due to the quality of picture cannot be analyzed by the software.

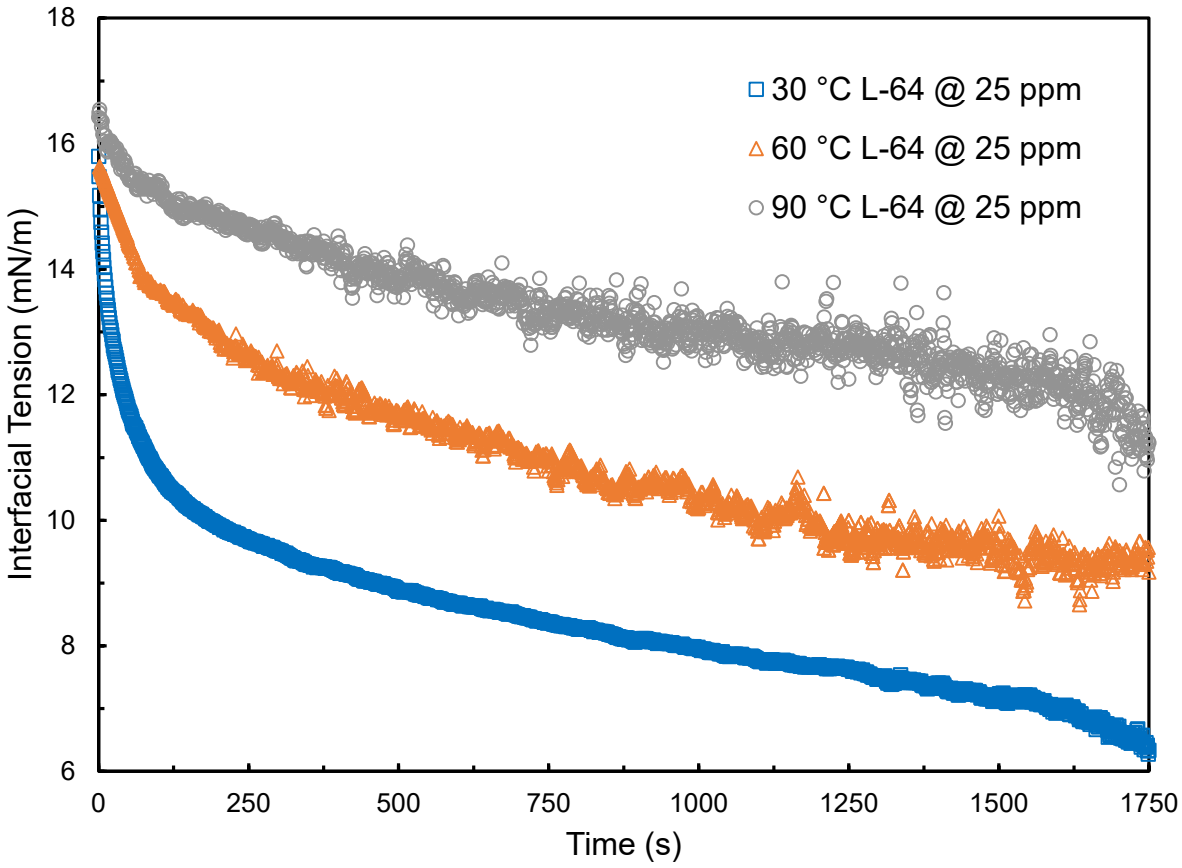

Figure 3. 8 Dynamic IFT vs time for 1000 ppm of asphaltene in toluene pendant drop in 25 ppm of Pluronic L-64 water solution at 30, 60 and 90 °C.

Regime I:

Same approaches were applied in Chapter 3.3.1: the dynamic IFT is plotted against the √t and the plot was generated in Figure 3.9. In this figure, three regimes were also observed and separated with dotted lines. Compared to previous experiment of 1000 ppm of asphaltenes pendant drop system without the addition of Pluronic L-64 surfactant, the surfactant reduces the dynamic IFT significantly for the first 250 seconds in both magnitude and rate at all 30, 60 and 90 °C. Interestingly, as the temperature increases, the reduction rate of dynamic IFT decreases. From the previous chapter, as the temperature increases, there are significant decreases in dynamic IFT. With the addition of 25 ppm of PEG-PPG-PEG polymer, the trends reversed totally opposite with asphaltene in toluene in pure water system.

For this interesting phenomenon, the effect of temperature on micellization may be explained: for ionic surfactant, micellization is surprisingly little affected by temperature considering that it is an aggregation process. However, non-ionic surfactants tend to show the opposite temperature effect: as the temperature raised, the cloud point may be reached at which large aggregates precipitate out into a distinct phase. By checking L-64 chemical properties, the 1 % and 10 % solution has a cloud point about 58 °C. As the temperature increased, water becomes a less good solvent for polyethylene glycol polymer. Therefore, at elevated temperature (60 °C and 90 °C), the turbid solution was observed in the pressure heating vessel, the rate change of IFT was not as pronounced as the lower temperature at 30 °C.

It is also interesting to note that 25 ppm of surfactants masked the effect of 1000 ppm of asphaltenes completely. In previous subchapter, with increasing temperature, the initial reduction of IFT was observed from 28 mN/m (30 °C) to 18 mN/m (120 °C) for 1000 ppm of asphaltenes solution. With the addition of merely 25 ppm of L-64, the initial IFT reduces to 16 mN/m regardless of the system temperature. The effect of chemical addition to reduce the IFT was very effective compared to the effect of increased asphaltenes concentrations.

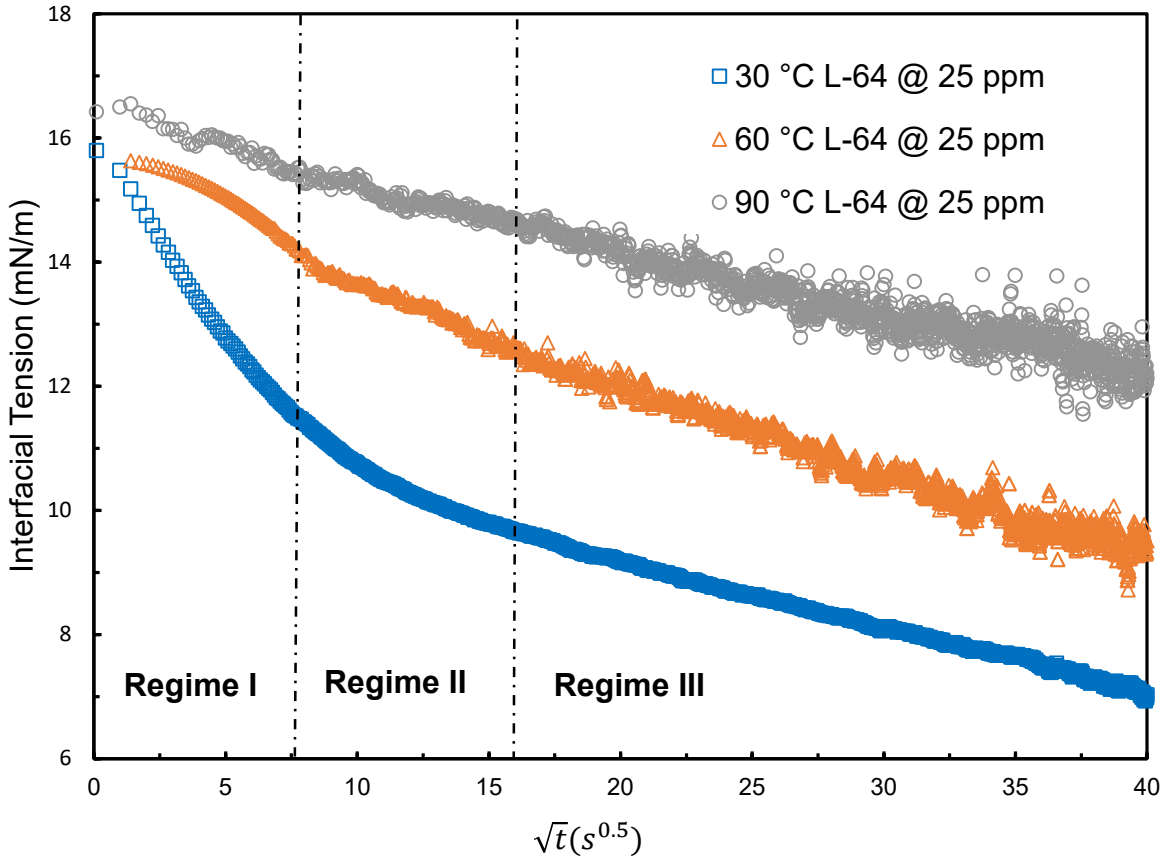

Figure 3. 9 Dynamic IFT vs √t for asphaltene in toluene pendant drop in 25 ppm of Pluronic L-64 water solution at 30, 60 and 90 °C.

Table 3. 3 Respective slopes and diffusion coefficients for Regime I for 1000 ppm of asphaltenes in 25 ppm of L-64 water solution at 30, 60 and 90 °C

	1000 ppm asphaltenes toluene pendant drop in 25 ppm of PEG-PPG-PEG water solution at 30 °C	1000 ppm asphaltenes toluene pendant drop in 25 ppm of PEG-PPG-PEG water solution at 60 °C	1000 ppm asphaltenes toluene pendant drop in 25 ppm of PEG-PPG-PEG water solution at 90 °C
Slopes	-0.562	-0.251	-0.153
Diffusion coefficient, D (m^2/s)	$3.90x10^{-14}$	$4.11x10^{-15}$	$2.02x10^{-15}$

Compared to 1000 ppm of asphaltene toluene in pure water system, the addition of 25 ppm of PEG-PPG-PEG polymer reduced the dynamic IFT significantly. From the IFT vs. √t plot, the slope in Regime I is -0.562 compared to -0.113 for asphaltene toluene/pure water system without surfactant addition. With the addition of Pluronic L-64 surfactant, the diffusion coefficient for the Regime I increases from $1.58x10^{-15}$ to $3.90x10^{-14}$, an order of magnitude larger. The PEG-PPG-PEG polymer dissolved in water formed a film immediately after the contact of asphaltene toluene droplet. The hydrophobic methyl group stick into the hydrophobic toluene droplet and formed sites for faster asphaltene adsorption.

As the temperature increases, one would assume that the diffusion coefficient of the asphaltene/toluene in surfactant/water solution could increase further. However, this is not the case. As the temperature increases from 30 to 60 °C, the diffusion coefficient reduces an order of

magnitude lower. As the temperature increase further to 90 °C, the diffusion coefficient decreased to half of that at 60 °C. Based on the experimental observation, at elevated temperature, the surfactant containing water will gradually become turbid. The asphaltenes adsorbed on the interface could be capsuled by the PEG-PPG-PEG polymer and emulsified as micelle in the water phase.

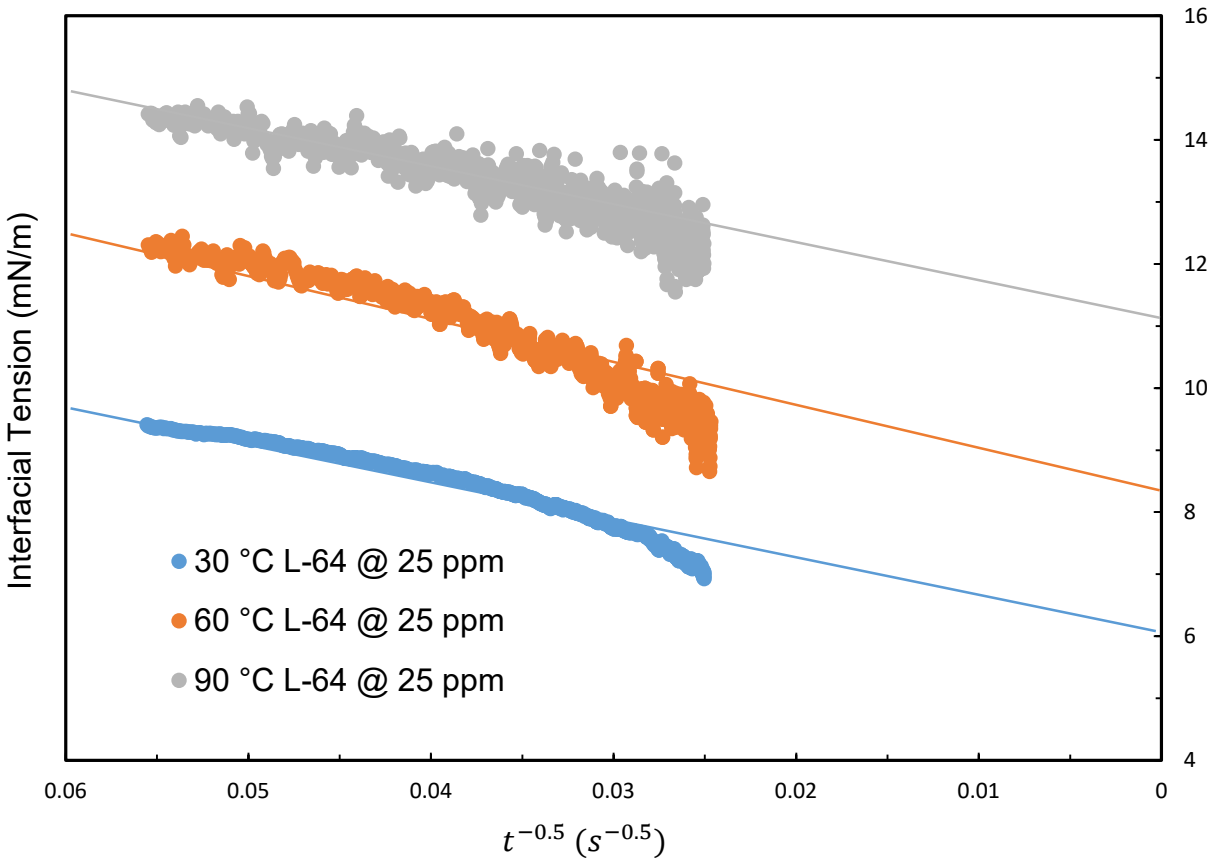

Figure 3. 10 Plots of γ_t vs. $t^{-0.5}$ in Regime III for 1000 ppm asphaltenes pendant drop in 25 ppm of Pluronic L-64 PEG-PPG-PEG water solution at 30, 60 and 90 °C (the x-axis is in reverse order).

Regime III: the extrapolations of $t^{-0.5}$ intercept with t=0 where equilibrium interfacial tension was obtained. The trend follows with IFT vs. time plot: as the temperature increases, the IFT

increases at a final equilibrium value. With the assistance of surfactants, the final equilibrium IFT decreases to an incredible low value of 6 mN/m compared to 24 mN/m at 30°C in previous chapter.

3.3.4 Effect of Aromaticity of Solvent for Asphaltenes Adsorption Process

For this subchapter, the effect of aromaticity of solvent with different volume composition of toluene and n-heptane was explored.

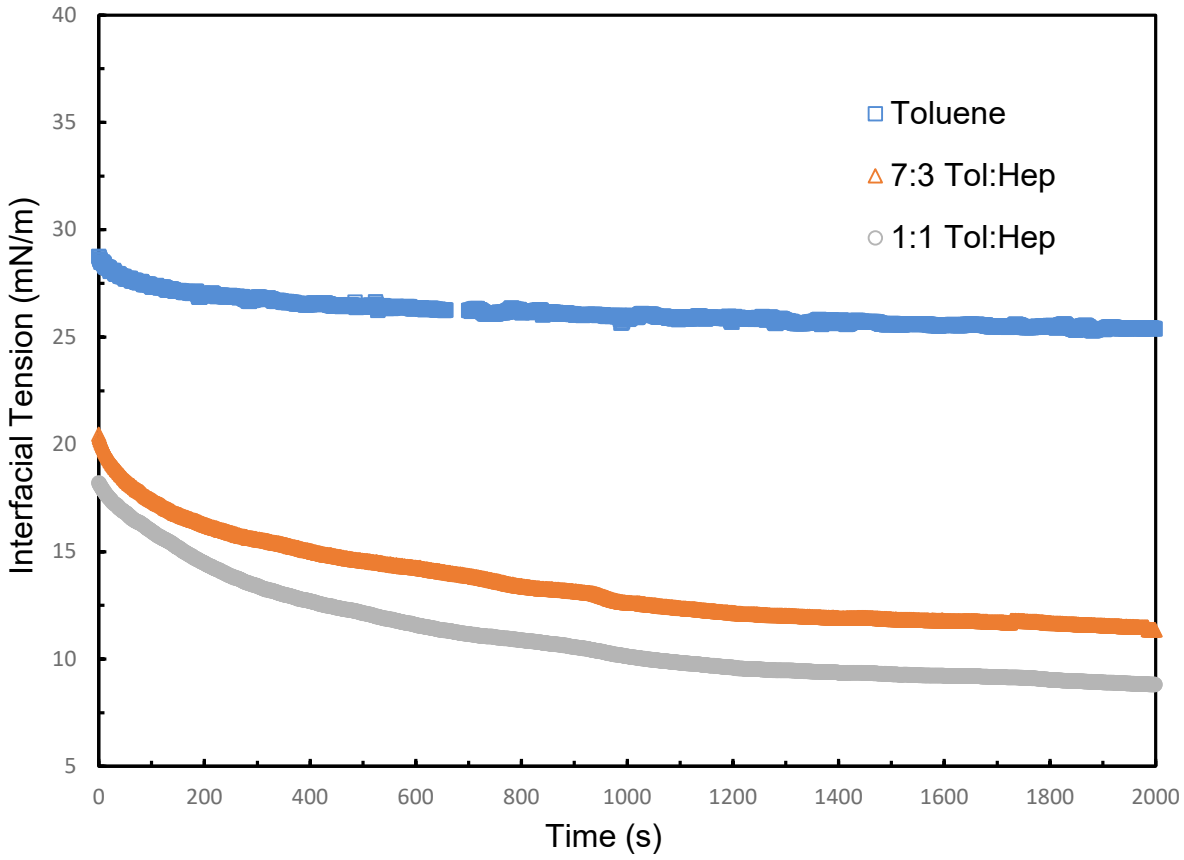

Figure 3. 11 Dynamic IFT vs. Time for 1000 ppm of asphaltene in toluene, 1:1 (v:v) toluene: heptane and 7:3 (v:v) toluene: heptane solution at 30 °C.

Same approaches were applied from previous chapter. For this chapter of experiment, 1000 ppm of asphaltene were dissolved in toluene, 7:3 (v:v) toluene: heptane (7:3 heptol) and 1:1 (v:v) toluene: heptane (1:1 heptol). Compared all three curves, the asphaltenes/toluene has highest IFT followed by 7:3 heptol and 1:1 heptol. For 7:3 and 1:1 heptol, the magnitude and decreasing rate of IFT are quite identical with just few units apart. In the following Figure 3.11, the IFT vs √t was plotted to show different regimes.

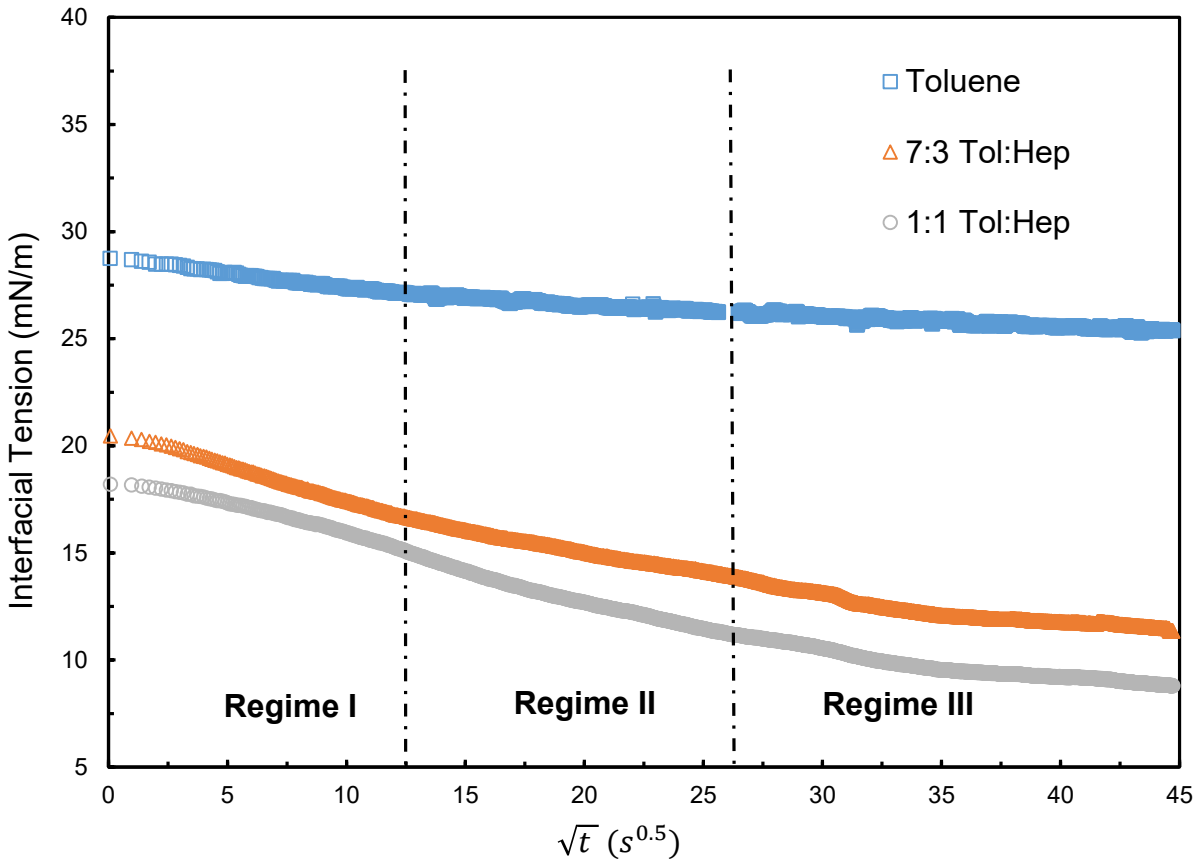

Figure 3. 12 Dynamic IFT vs. √t for 1000 ppm asphaltenes pendant drop in toluene, 7:3 (v:v) toluene:heptane, and 1:1 (v:v) toluene:heptane solution in water system at 30 °C.

Regime I: From Figure 3.12, the plot of IFT vs. √t has shown three regimes as described in previous chapter. Compared to asphaltenes/toluene system, the 7:3 heptol reduced the IFT significantly from 25 ~ 30 mN/m range to 10 ~ 20 mN/m range. With more heptane added into the asphaltenes/heptol system, further reduction of IFT was observed but with a fraction of improvement for 1:1 heptol solution.

Table 3. 2 Respective slopes and diffusion coefficients for Regime I for 1000 ppm of asphaltenes pendant drop in toluene, 7:3 (v: v) and 1:1 (v: v) toluene:heptane in water at 30°C.

	1000 ppm asphaltenes in toluene	1000 ppm asphaltenes in 7:3 (v:v) toluene: heptane	1000 ppm asphaltenes in 1:1 (v:v) toluene: heptane
Slopes	-0.113	-0.316	-0.305
Diffusion coefficient, D (m^2/s)	$1.58x10^{-15}$	$1.23x10^{-14}$	$1.15x10^{-14}$

For the Regime I, the slope of asphaltenes in different solvents were calculated. Then the diffusion coefficients were also calculated. Compared to asphaltenes/toluene system, significant increases in diffusion coefficient were observed with 7:3 and 1:1 heptol system with an order of magnitude increase. As the heptane is a "poor solvent" for large molecular weight aromatic asphaltene compound, the asphaltene molecules are likely precipitate out and adsorbed onto the solvent/water interface. By decreasing the aromaticity of the solvent system to 1:1 ratio, the diffusion coefficient almost remains unchanged.

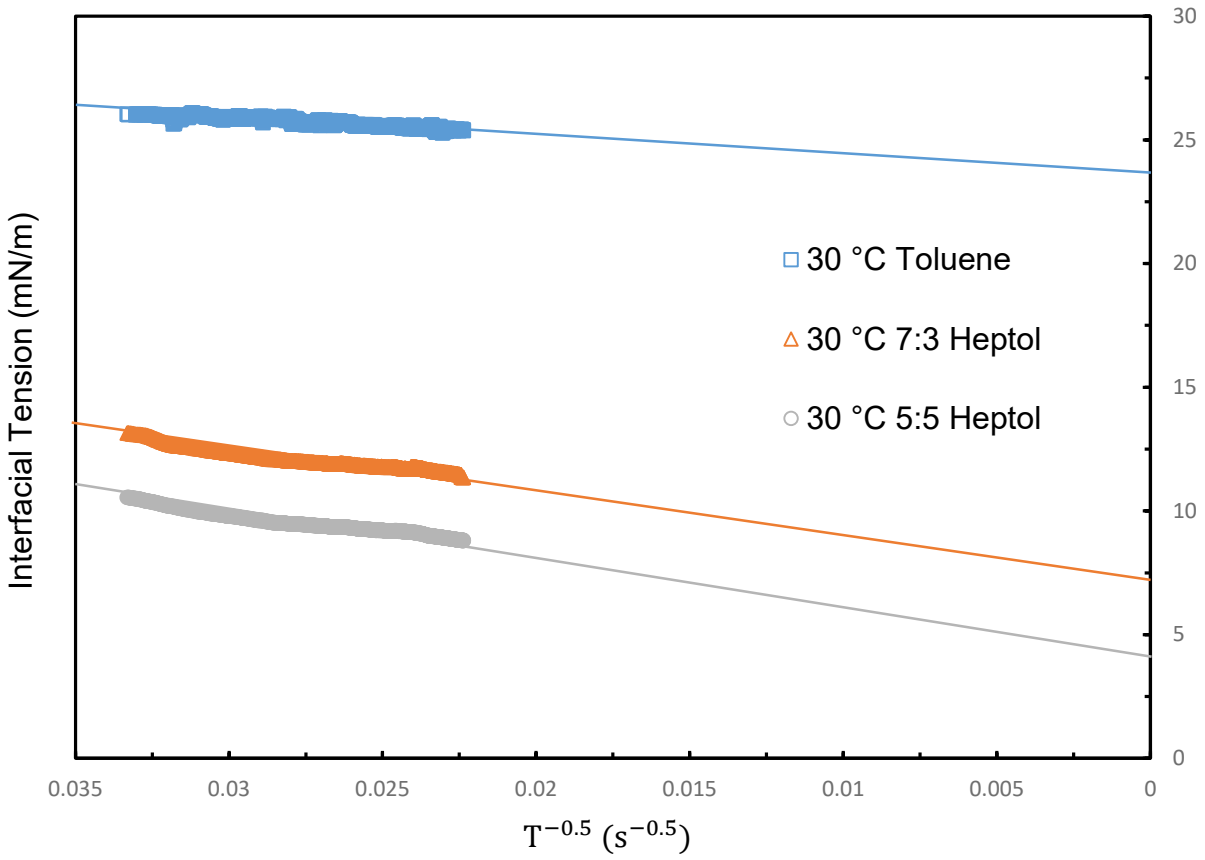

Figure 3. 13 Plots of γ_t vs. $t^{-0.5}$ in Regime III for 1000 ppm asphaltenes in toluene, 7:3 Heptol and 1:1 heptol pendant drop in water solution at 30 °C (the x-axis is in reverse order).

Regime III: For this plot, the equilibrium dynamic IFT was determined by the intercept of Y axis. Compared to pure aromatic solvent based asphaltenes solution, the aliphatic solvent reduces the IFT significantly to 7 and 4 mN/m respectively with more reduction with more heptane content.

3.4 Conclusions

In this study, the adsorption kinetics of asphaltene at oil/water interface were investigated by analyzing dynamic IFT using pendant drop shape method. Effect of system temperature from 30 to 120 °C, addition of surfactant and composition of solvent were analyzed. Three regimes were

found during the adsorption process. Regime I was dominated by short term diffusion-controlled process. Regime III was dominated by long term adsorption process. Regime II was a transitional regime between regime I and III. For the effect of temperature, it was found that as the temperature increases, the dynamic IFT decreases gradually. With addition of PEG-PPG-PEG surfactant, the dynamic IFT decreases significantly. However, as the temperature increases with addition of surfactant, the effect was reversed due to possible reduced surfactant solubility. By changing the aromaticity of the solvent system, it was found that gradual addition of aliphatic solvent reduces the dynamic IFT significantly. To conclude, the study simulates a series of conditions approximated to industrial operating conditions such as elevated temperature, addition of surfactant and the blending of available solvent.

Reference

(1) Podgorski, D. C. (2013). "Heavy Petroleum Composition. 5. Compositional and Structural Continuum of Petroleum Revealed". *Energy & Fuels*. 27 (3): 1268–1276. doi:10.1021/ef301737f.

(2) Speight, J.G., *The chemistry and technology of petroleum*, 3rd edition.; Marcel Dekker: New York, 1999; p xiv, 918p.

(3) Mullins, O.C., *Asphaltenes, heavy oils, and petroleomics*. Springer: New York, 2007; p xxi, 669p.

(4) Spiecker, P. M.; Kilpatrick, P. K., Interfacial rheology of petroleum asphaltenes at the oil-water interface. *Langmuir* **2004,** *20*, 4022-4032.

(5) Nguyen, D.; Balsamo, V.; Phan, J., Effect of Diluents and Asphaltenes on Interfacial Properties and Steam-Assisted Gravity Drainage Emulsion Stability: Interfacial Rheology and Wettability. *Energy & Fuels* **2014,** *28*, 1641-1651.

(6) Pauchard, V.; Rane, J. P.; Banerjee, S., Asphaltene-laden interfaces form soft glassy layers in contraction experiments: a mechanism for coalescence blocking. *Langmuir* **2014,** *30*, 12795-803.

(7) Pauchard, V.; Roy, T., Blockage of coalescence of water droplets in asphaltenes solutions: A jamming perspective. *Colloids and Surfaces A: Physicochemical and Engineering Aspects* **2014,** *443*, 410-417.

(8) Samaniuk, J. R.; Hermans, E.; Verwijlen, T.; Pauchard, V.; Vermant, J., Soft-Glassy Rheology of Asphaltenes at Liquid Interfaces. *Journal of Dispersion Science and Technology* **2015,** *36*, 1444-1451.

(9) Bouriat, P.; El Kerri, N.; Graciaa, A.; Lachaise, J., Properties of a two-dimensional asphaltene network at the water - Cyclohexane interface deduced from dynamic tensiometry. *Langmuir* **2004,** *20*, 7459-7464.

(10) Jennings, H. Y. JR.; "The effect of temperature and pressure on the interfacial tension of benzene-water and normal decane-water." *Journal of collid and interface science,* **1967,** 24, 323 – 329.

(11) Rane, J. P.; Harbottle, D.; Pauchard, V.; Couzis, A.; Banerjee, S.; "Adsorption kinetics of asphaltenes at oil-water interface and nanoaggregation in the bulk." *Langmuir,* **2012**, 28 (26), 9986 – 9995.

(12) Hu, C.; Garcia, N. C.; Xu, R.; Cao, T.; Yen, A.; Garner, S. A.; Macias, J. M.; Joshi, N.; Hartman, R. L., Interfacial Properties of Asphaltenes at the Heptol–Brine Interface. *Energy & Fuels* **2016,** *30*, 80-87.

(13) Czarnecki, J.; Moran, K., On the stabilization mechanism of water-in-oil emulsions in petroleum systems. *Energy & Fuels* **2005,** *19*, 2074-2079.

(14) He, Kai, Christina Nguyen, Ramya Kothamasu, Liang Xu, and others. "Insights into Whether Low Salinity Brine Enhances Oil Production in Liquids-Rich Shale Formations." *EUROPEC 2015*. Society of Petroleum Engineers, 2015.

(15) Silva Ramos, Antônio Carlos da, Lilian Haraguchi, Fábio R. Notrispe, Watson Loh, and Rahoma S. Mohamed. "Interfacial and Colloidal Behavior of Asphaltenes Obtained from Brazilian Crude Oils." *Journal of Petroleum Science and Engineering* 32, no. 2 (**2001**): 201–216.

(16) ASTM D6560-17, Standard Test Method for Determination of Asphaltenes (Heptane Insolubles) in Crude Petroleum and Petroleum Products, *ASTM International*, West Conshohocken, PA, 2017

(17) Beverung, C. J.; Radke, C. J.; Blanch, H. W., Protein adsorption at the oil/water interface: characterization of adsorption kinetics by dynamic interfacial tension measurements. *Biophys Chem* **1999,** *81*, 59-80.

(18) Sheu, E. Y., Petroleum asphaltene-properties, characterization, and issues. *Energy & Fuels* **2002,** *16*, 74-82.

(19) Li, Z. F.; Geisel, K.; Richtering, W.; Ngai, T., Poly(N-isopropylacrylamide) microgels at the oil-water interface: adsorption kinetics. *Soft Matter* **2013,** *9*, 9939-9946.

(20) Giusti, F.; Popot, J. L.; Tribet, C., Well-defined critical association concentration and rapid adsorption at the air/water interface of a short amphiphilic polymer, amphipol A8-35: a study by Forster resonance energy transfer and dynamic surface tension measurements. *Langmuir* **2012,** *28*, 10372-80.

(21) Benjamins, J., J. A. De Feijter, M. T. A. Evans, D. E. Graham, and M. C. Phillips., Dynamic and Static Properties of Proteins Adsorbed at the Air/water Interface. *Faraday Discussions of the Chemical Society* **1975**.

(22) Graham, D. E.; Phillips, M. C., Proteins at Liquid Interfaces .1. Kinetics of Adsorption and Surface Denaturation. *Journal of Colloid and Interface Science* **1979,** *70*, 403-414.

(23) Pauchard, V.; Rane, J. P.; Zarkar, S.; Couzis, A.; Banerjee, S., Long-term adsorption kinetics of asphaltenes at the oil-water interface: a random sequential adsorption perspective. *Langmuir* **2014,** *30*, 8381-90.

(24) Poteau, S.; Argillier, J. F.; Langevin, D.; Pincet, F.; Perez, E., Influence of pH on stability and dynamic properties of asphaltenes and other amphiphilic molecules at the oil-water interface. *Energy & Fuels* **2005,** *19*, 1337-1341.

(25) Yarranton, H. W.; Alboudwarej, H.; Jakher, R., Investigation of asphaltene association with vapor pressure osmometry and interfacial tension measurements. *Industrial & Engineering Chemistry Research* **2000,** *39*, 2916-2924.

Chapter 4 Dilatational Interfacial Properties: Effect of Temperature, Concentration of Asphaltenes and Ionic Strength

4.1 Introduction

Steam-assisted gravity drainage (SAGD) is a thermal enhanced oil recovery process in which steam is injected into the ground continuous to extract heavy oil or bitumen from underground. Due to the nature of Northern Alberta oil reserves, there are plenty of oil producers are currently either adopting, planning, or designing with this process. In this process, 3 barrels of water equivalent of steam is used to recovery 1 barrel of bitumen. Therefore, large quantity of produced water is generated in this process and resulting a very complex water-in-oil-in-water (W/O/W) emulsions [1]. SAGD process offers several advantages in comparison to oil sands surface mining process including less surface disturbance and less water usage. However, the biggest drawback when dealing with SAGD emulsions is the high viscosity of bitumen and similar density with water which makes more difficult for gravity separation [2].

The SAGD emulsions have been widely accepted that emulsions are stabilized by surface active asphaltenes and resin particles. Asphaltenes are defined as the solubility class of crude oils which precipitate in the presence of aliphatic n-heptane, n-hexane or n-pentane solvent. Resins are heavier than aromatics and saturates but lighter than asphaltenes. They are soluble in heptane but insoluble in liquid propane. Asphaltenes and resins are large polar and polynuclear molecules with condensed aromatic ring molecules also containing heteroatoms and metal atoms such as nitrogen, oxygen, sulphur, nickel and vanadium. According to Yen-Mullins model, asphaltene molecules

will self-associate and form nanoaggregates, with the aggregation number usually less than 10, as a result of π-π interaction between condensed aromatic rings. Clusters will be further formed by nanoaggregates because of the crosslinking of aliphatic chains [3].

Over the decades, extensive studies were linking the emulsion stability to the properties of oil and water interface properties such as interfacial tensions and interfacial rheology. Due to the complexity of crude oils, simple modular systems are usually used to study the roles of asphaltenes played in stabilizing emulsions [4]. A number of studies have been focused on the effect of aging time on the IFT [5-10], concentration of asphaltenes [5-8, 11-15], categorized asphaltenes by extraction method such as n-pentane and n-heptane [16], polarity of solvent [8, 10, 17], ratio of resin/asphaltene [8, 11, 18, 19], temperature/pressure of the oil/water system [14,16, 20, 21] and pH value of the aqueous phase [22-24].

There have been lots of researched done from different perspectives. However, few of them explore the possibility of performing the experiment at elevated temperature and pressure. In SAGD process, complex oil-in-water-in-oil emulsions are generated by tremendous agitation from the steam and pumping action. Then the fluid transported in several kilometer of pipelines into the first separator vessel, as known as Free Water Knock Out (FWKO) vessel. Before the emulsion entering the FWKO, the reverse emulsion breakers (water clarifier), diluent, and demulsifiers are added to enhance the separation process. In FWKO, the separation process is happened at 120 ~ 140 °C. At this temperature, the water and diluent need to be under specific pressure in order to keep them in liquid state for separation. In the field operation, this pressure is usually in the range of 340 kPa to 1400 kPa due to vapor pressure imposed by the components in the diluents. In this study, a pressure vessel with heating capability was used to increases the temperature to a

maximum of 120 °C and pressure up to 340 kPa. At this pressure and temperature, our model system comprised of toluene and water remains at liquid state.

It was well recognized that the water-in-oil emulsions behavior is controlled by the properties of the amphiphilic film that formed between water droplets in crude oil interfaces. The interfacial tension gradient is induced by resins and asphaltenes, which mainly compose the interfacial film. They behave like an elastic film to prevent coalescence therefore create problems down stream processing [25-27]. Much research has been conducted in order to associate interfacial rheological properties with emulsion behaviors. Several techniques have been used on different measurement: with a drop dilation/compression oscillatory tensiometers [10, 28-33]; with a flat interface by means of rotating/oscillatory interfacial device [34-36]. Most these studies were using model oil and water system. With some of the additives applied such as demulsifiers in order to understand the chemical process [37, 38]. Strong correlations between interfacial viscoelastic properties and emulsion stability has been confirmed.

Among these studies, it has been found that the solution of asphaltenes formed a two-dimensional gel at the oil/water interface [29]. The theories were in first developed by Chambon and Winter that the asphaltene matrix formed a cross linked gel. This behavior is also true for a diluted crude oil and a diluted heavy fraction of same crude oil. It is also observed that the gel formation is possible even in the absence of asphaltenes. [39, 40]

Several researches were focused on the correlation between aged time of the film with the viscoelastic behavior. It has been concluded that the older is the oil/water interface, more stable is the emulsion system [41]. Hence, the elastic moduli increase with film aged time. In the Chapter 3 of this study, it is also confirmed that for the kinetics of film formation, the rate of change in

interfacial tension varies with different process conditions. The ability of some amphilic molecules to rapidly adsorb may induce the formation of a rigid film since very short times and determine the emulsion stability [42].

When inorganic salts are present in the aqueous solution, the water molecules from a cage-like hydrogen bonded structure around the salt ions. At the interface, the salts are depleted near the interface and the surface excess concentration is negative. As predicted by the Gibbs adsorption isotherms with multi components system, interfacial tension increases when surface excess concentration is negative.

The effect of temperature on dilatational rheology of deionized water and toluene system at 120 °C was experimented as our baseline study. Then, the dilatational rheology of asphaltene solutions with different concentration in toluene were analyzed. Finally, the dilatational rheology of asphaltenes solution in saline water at different concentration (ionic strength) was analyzed.

4.2 Materials and Methods

4.2.1 Materials

In this study, Milli-Q water (resistance of ≥18.2 MΩ·cm) was used to prepare all aqueous solutions. ACS grade of Toluene were purchased from Fisher Scientific Canada. Sodium chloride was purchased from Sigma Aldrich Canada.

4.2.2 Asphaltene sample preparation

Bitumen sample was obtained from a SAGD facility. The sample was first purified by Dean Stark Extraction process according to ASTM D6560 procedure [43] using toluene reflux. Then the purified bitumen toluene solution was concentrated, toluene was removed from the bitumen in the oven. The purified bitumen was then thoroughly mixed with n-heptane with 1:1 ratio and finally diluted to 40:1 n-heptane to bitumen ratio in order to precipitate maximum amount of asphaltenes. Asphaltenes particles were filtrated and washed with n-heptane to remove any bitumen residue. Finally, the asphaltene sample were dried, ground into powder and store in desiccator before use.

4.2.3 Interfacial dilatational rheology test

The same Ramé-hart tensiometer equipped with oscillator was used for this group of experiment. The oscillator has a glass syringe and a metal syringe piston with PTFE seal. The piston is attached to an actuator for sinusoidal movement. For oscillator, the amplitude of the oscillation was adjusted manually to 0.6 uL to successfully adhere the droplet on the syringe tip. The volume of the oscillation amplitude is controlled at 10 % of total volume of the drop. Large oscillation volume can cause the droplet to dislodge from the syringe tip. The oscillation frequency is set to 0.1, 0.25, 0.5, 0.75 and 1.0 Hz. Compared to previous researcher's work, the oscillation frequency is only limited to 0.005 to 0.2 Hz. This test explored more on the high frequency of the oscillation. It was

worth mentioning that the capability of instruments depends on the mechanical movement of the oscillator as well as the maximum frame rate of high-speed camera. As the frequency increases, one can expect the quality of the measurement may decrease. Future improvement on the instrument are mentioned in the final section of this thesis.

4.2.4 Data Analyses and tan φ Conversion

After each dilatational rheology oscillation, the ramé-hart software generates a texted result file. The results were copied into Microsoft Excel for data analyses. The following Table 4.1 shows a typical data converted into Excel format.

Table 4. 1 A typical dilatational oscillation results generated by ramé-hart software.

No.	A0 (mm^2)	A(amp) (mm^2)	Gamma (mN/m)	G(amp) (mN/m)	Fi2 (radians)	E′	E′′	tg(d)	A/G
Test Number	Mean Surface Area	Area Amplitude	Mean Surface Tension	Surface Tension Amplitude	Shift in Surface Tension	Storage Modulus	Viscous Modulus	Damping factor	Ratio of A(amp)/G(amp)
1	43.85	1.42	28.74	0.22	-1.268	6.64	-1.66	-0.25	6.41
2	43.93	1.42	28.67	0.23	-1.16	6.9	-1.43	-0.207	6.231
3	43.9	1.43	28.56	0.22	-1.107	6.79	-1.11	-0.164	6.376
4	43.87	1.42	28.56	0.24	-1.132	7.26	-1.18	-0.162	5.968
5	43.85	1.42	28.46	0.24	-1.153	7.25	-1.29	-0.178	5.952

Note that both E” and tan φ written as tg(d) in the table are in negative values. After consulting with ramé-hart software developer and programmer, the negative value for phase angle (phase

shift) could be generated by the software artifact and can be corrected with their respective absolute value.

4.3 Theory and Experimental on measuring surface dilatational modules

The theoretical foundation for measuring surface rheological properties has been well established. The analysis of surface dilatational elasticity and viscosity has been reviewed by Lucassen-Reynders. In this work, the theoretical background and methods are outline below. The surface elasticity, E, follows the definition given by Gibbs

$$E = \frac{d\gamma}{d \ln A} \tag{4.1}$$

Where γ is the surface tension and A is the surface area. The term surface elasticity infers that E is a property of pure elastic surfaces. However, for many cases, the surfaces both contain elastic and viscous components and the term "surface dilatational modulus" has been used for this more general case. The contribution of the elastic and viscous terms depends on the different types of relaxation processes that occur in the surface layer and on the interaction of the surface with its surroundings, i.e. the bulk liquid. The equilibrium Gibbs surface elasticity, E_0, will then usually be different from E. The surface dilatational viscosity, η_d, has been defined according to the equation:

$$\Delta\gamma = \eta_d \frac{d \ln A}{dt} \tag{4.2}$$

Where Δγ is the surface tension difference of a constantly logarithmically expanding surface compared to that of the equilibrium surface. The parameter η_d will only represent true Newtonian types of surface viscosity, however, if the elasticity is zero. In other cases, a complex surface dilatational modulus may be written as

$$E^* = E' + iE'' \tag{4.3}$$

Where E' is the storage or elastic modulus and E" is the loss or viscous modulus. The storage modulus will be equal to the pure elastic contribution, and E" is proportional to the viscous contribution. The total modulus represents a change in the energy of the system with a corresponding change in area. The elastic modulus can be thought of as the energy store in the system, and the viscous modulus as the loss energy. The elastic and viscous moduli can be expressed as total modulus, $|E|$, and the phase angle, φ, as follows:

$$E' = |E|cos\varphi \tag{4.4}$$

And

$$E'' = \omega\eta_d = |E|\sin\varphi \tag{4.5}$$

The viscous modulus is the product of the frequency of oscillation, ω, and the interfacial viscosity, η_d.

4.4 Results and Discussions

4.4.1 Interfacial Dilatational Rheology of Toluene/Water System at 30, 60, 90 and 120 °C

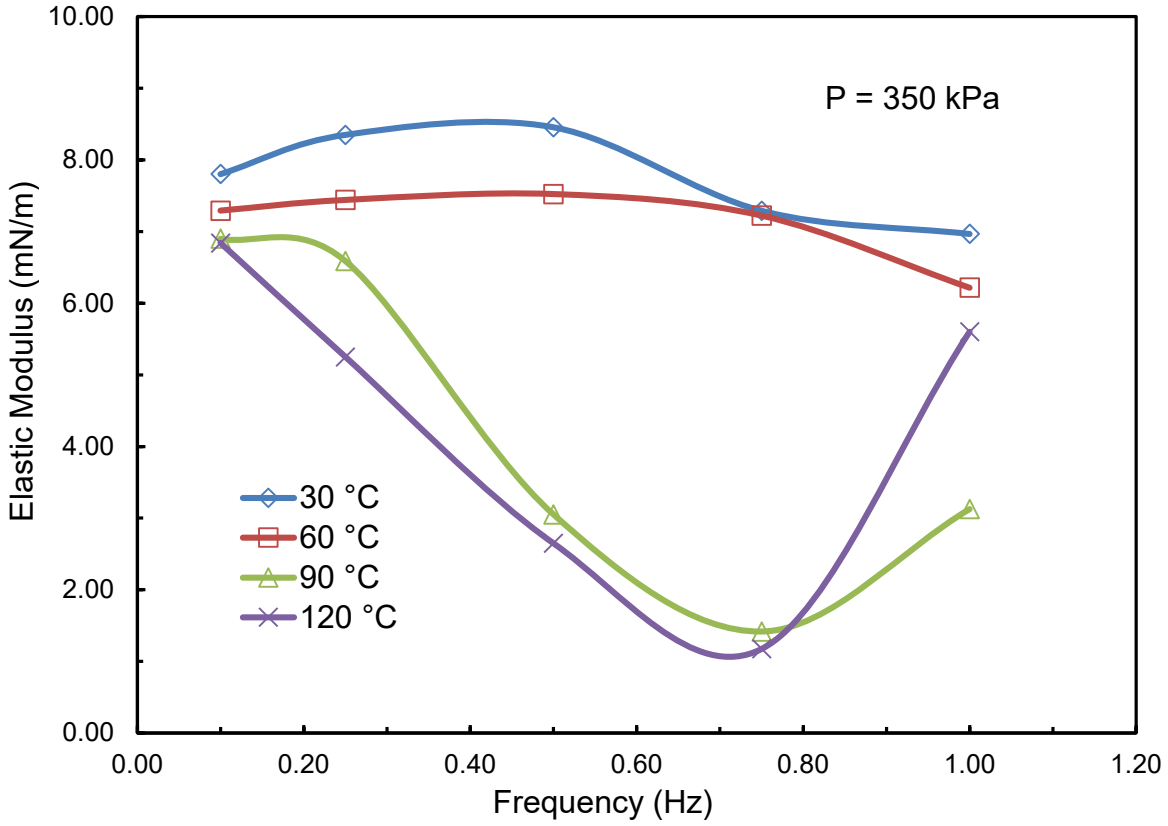

Figure 4. 1 Effect of oscillation frequency on elastic moduli in the system of toluene in water over a range of 0.1 Hz to 1.0 Hz at 30, 60, 90 and 120 ºC. The curves are visual aids only.

First, a blank system of toluene/water was tested to establish the baseline. The instrument was thoroughly cleaned and rinse with toluene followed with acetone and then water to remove any oil or surfactant residue may be present in the system. With each fresh toluene drop suspended in the water, 10 minutes of aging time was given thorough out the experiment.

For this subchapter, the effect of oscillation frequency and temperature were explored. Frequency is one of the most important indictors investigated by many researchers. Most of the research were focused on lower frequency region from 0.01 Hz to 0.1 Hz. However, in this study, the frequency varied from 0.1 Hz to an order of magnitude higher at 1.0 Hz. For 30 °C and 60 °C elastic curves, it was observed that as the frequency increased from 0.1 Hz to 0.5 Hz, the elastic moduli increases slightly. Above 0.5 Hz, the elastic moduli decreased slightly and were in same level at 0.1 Hz. At 0.1 Hz, as the temperature increased gradually from 30 °C to 120 °C, every 30 °C of temperature change decrease the elastic moduli about 0.4 mN/m. For 90 °C and 120 °C, the slight increase of elastic moduli was not observed from region of 0.1 Hz to 0.5 Hz. Instead, rapid decrease of elastic moduli was observed. Both curves show that at 0.75 Hz, the elastic moduli were reduced to 1 ~ 1.5 mN/m. At higher frequencies, the values of elastic moduli seem to be random. From Quintero's work, it has been found that for the higher oscillation values, elastic moduli become almost independent of the frequency for frequency > 0.1 Hz [44].

This strong evidence indicated that as the temperature increases, the moduli for pure toluene and water interface decreases. Hence, at elevated temperature, the toluene/water interface was softened, and the emulsion stability decreases. This explained that for certain oil purification process such as SAGD operation, an elevated temperature was highly desirable simply because of weakened emulsion stability.

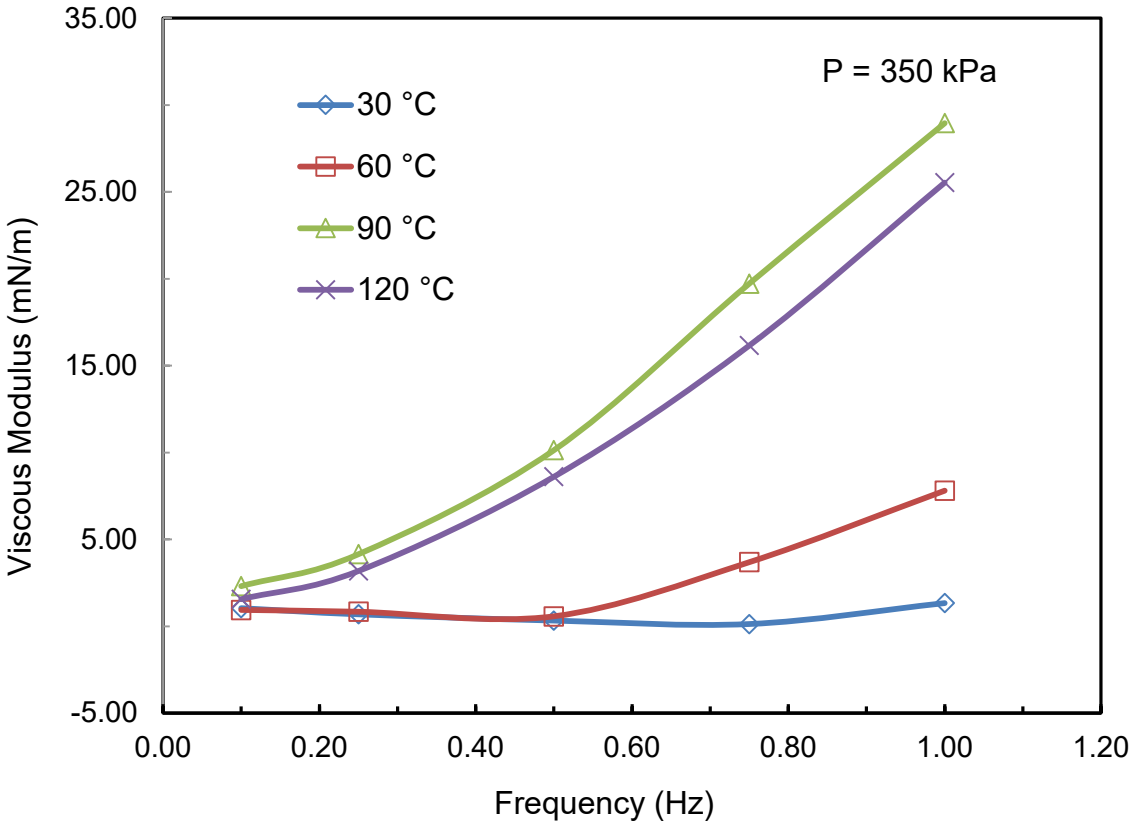

Figure 4. 2 Effect of oscillation frequency on viscous moduli in the system of toluene in water over a range of 0.1 Hz to 1.0 Hz at 120 ºC. The curves are visual aids.

For 30°C viscous modulus curve, it started at about 1 mN/m. As the frequency increased, it remains at same level through the range between 0.1 Hz to 1.0 Hz. Compared to 30 °C curve, the 60°C modulus curve shows this trend with augmented effect: as the temperature increased, the viscous moduli increased gradually with significant change above 0.75 Hz to 8 mN/m. For 90 °C and 120 °C curves, both curves exhibited similar trends with significant increase on viscous moduli with increased oscillation frequencies. They increased to 29 and 25 mN/m respectively at 1.0 Hz. The difference between the two curves are much less compared to the differences between those curves of 60 °C and 90 °C. One can conclude that with increased temperature, the viscous moduli

increase significantly for toluene/water interface. In addition, at higher temperatures, viscous moduli increase much more with higher oscillation frequencies.

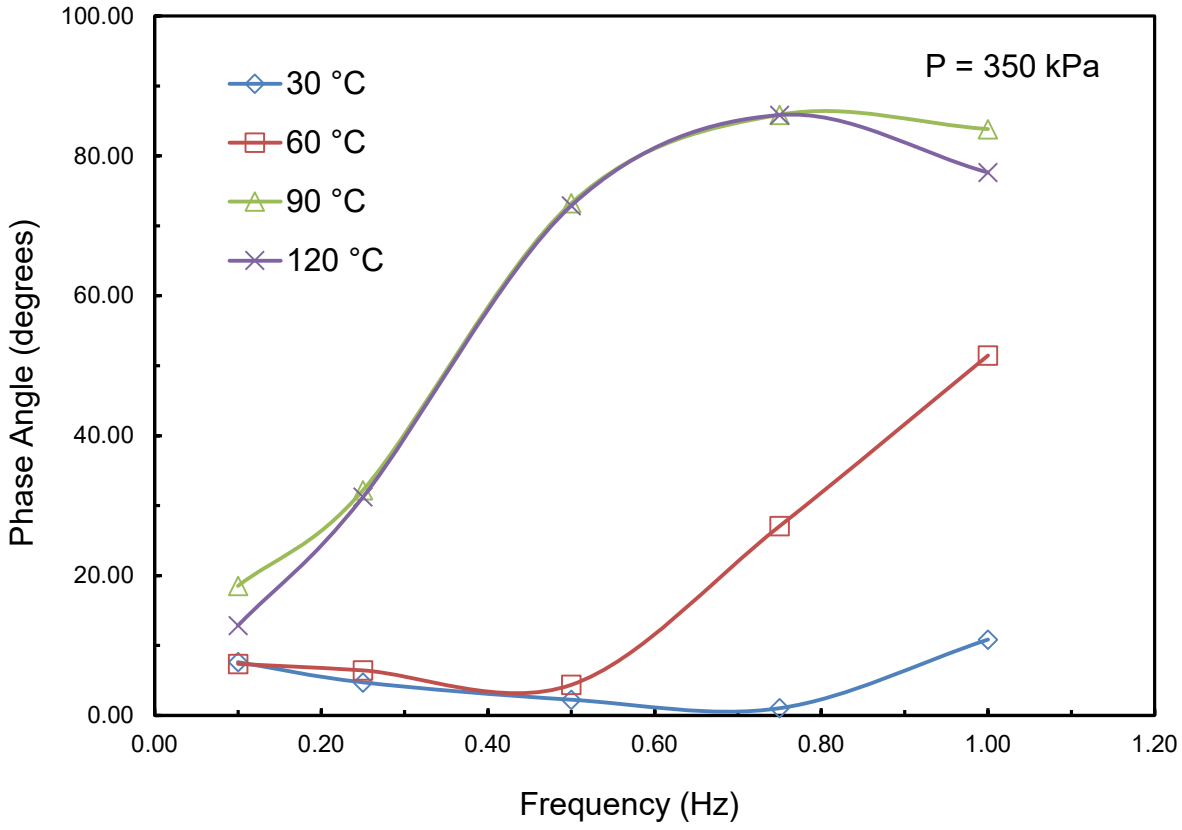

Figure 4. 3 Effect of oscillation frequency on phase angles in the system of toluene in water over a range of 0.1 Hz to 1.0 Hz at 120 ºC. The curves are visual aids.

The phase angle which is the time lag between the pre-set and the resulting sinusoidal oscillation is determined for each measuring point. This angle is always between 0 ° and 90 °. For the solid, gel-like state, the phase angle is between 0 ° and 45 °. For the fluid state, the phase angle is between 45 ° and 90 °. Phase angle represents a combination of elastic and viscous moduli. For 30 °C profile, as the oscillation frequency increases, the phase angle remains less than 10 ° which

indicates that at low temperature, the toluene/water interface remain relatively rigid. With increased temperature and increased oscillation frequency, the phase angle increases to near 45 °, hence, more liquid state. At 90 and 120 °C, with 0.5 Hz of oscillation frequency, the phase angle increases above 70 °. One can conclude that the interface between toluene and water behaves more as a viscoelastic liquid. With higher temperature and higher frequency, more viscoelastic liquid property was demonstrated.

4.4.2 Interfacial Dilatational Rheology of 1000 ppm of Asphaltenes in Toluene vs. Water System at 30, 60, 90 and 120 °C

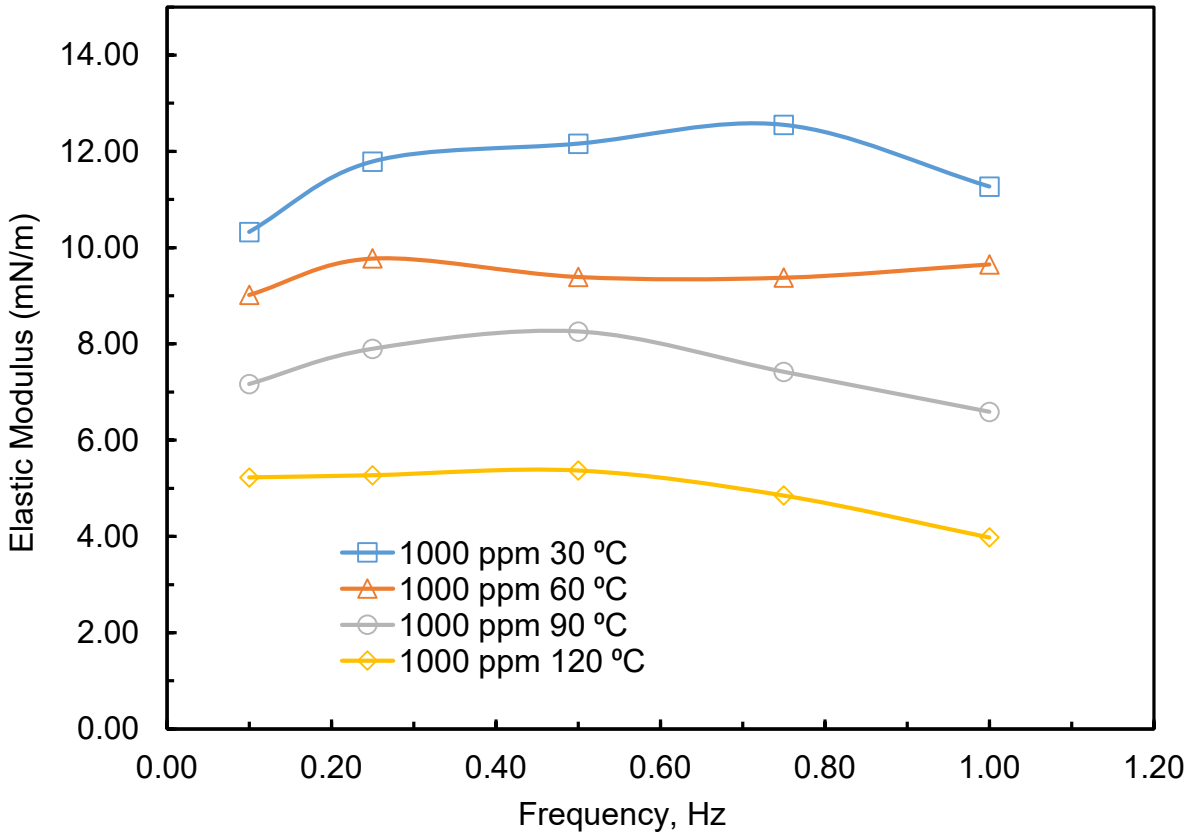

Figure 4. 4 Effect of different temperature on elastic modulus for 1000 ppm of asphaltene/toluene pendant drop vs. frequency in water at 30, 60, 90 and 120 °C. Curves are visual aids only.

The same test was repeated with 1000 ppm of asphaltenes in toluene pendant drop in water at different temperatures. Compared to toluene/water system in the previous subchapter, 1000 ppm of asphaltenes/toluene in water system at 30 °C has slightly higher elastic moduli above 10 mN/m. Compare all three temperature curves, increased temperatures reduce the elastic moduli by 1.5 mN/m per 30 °C of change. From Chapter 3, it has been observed that as the temperature increases, the dynamic IFT decreases with increased diffusion coefficient. It is easy to observe that as the temperature increases, the diffused asphaltenes film onto the toluene/water interface was softened as the elastic moduli decreased. With the frequency increases, the elastic moduli did not decrease much as the behavior displayed with pure toluene/water (or simply independent of higher frequencies). Adsorbed asphaltenes formed semi-rigid layer to maintain solid-like behavior of asphaltenes pendant drops.

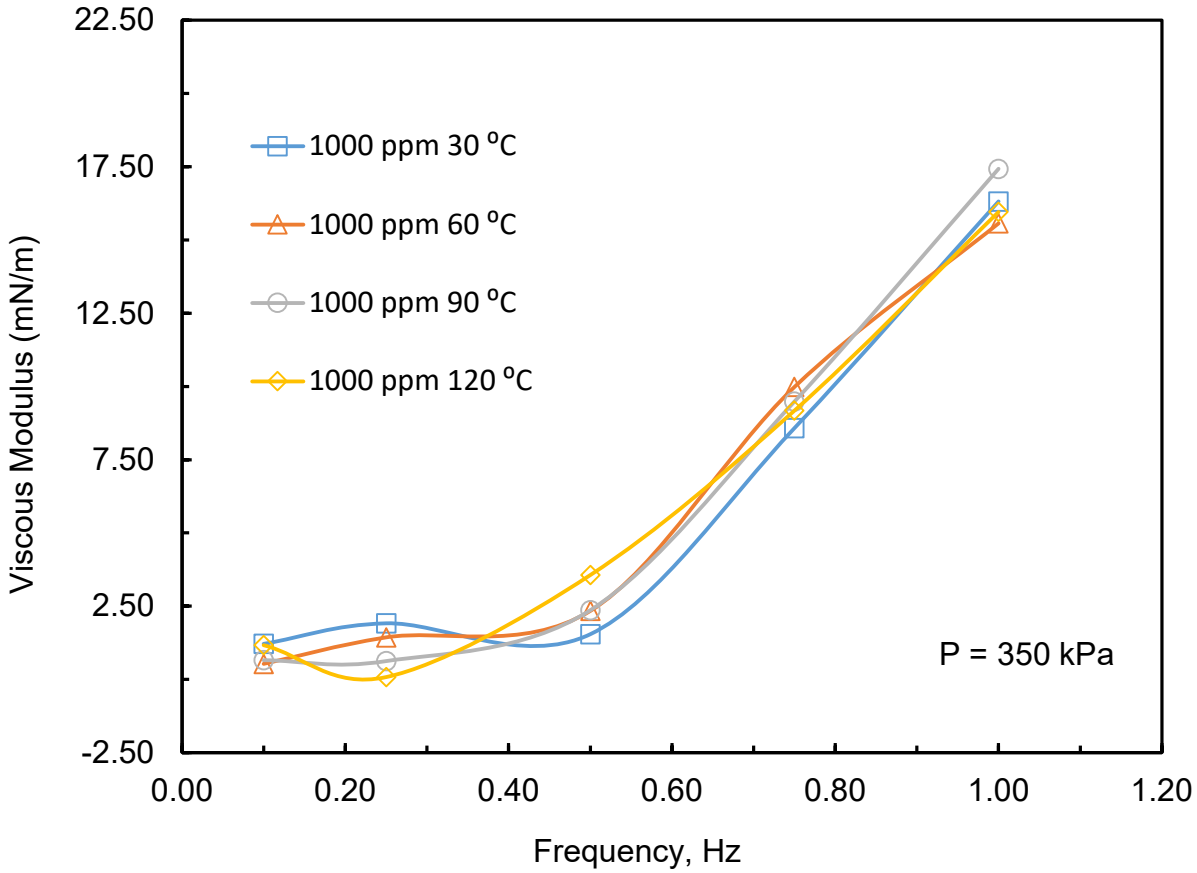

Figure 4. 5 Effect of temperature on viscous moduli of 1000 ppm of asphaltenes/toluene pendant drop in water at 30, 60, 90 and 120 °C. Curves are visual aids only.

With 1000 ppm of asphaltenes from 30 °C to 120 °C, the viscous moduli look almost identical. As the frequency increases, the viscous moduli gradually increase from 1 to 15 mN/m. Compared to pure toluene and water system, there is drastic difference: for toluene/water system, as the temperature increases, the viscous moduli increase significantly. In other word, the asphaltene film formed between the toluene/water interface is insensitive to temperature change. The elasticity of the asphaltene film does reduce as the temperature increases, but the viscosity of the asphaltene films is independent of the temperature variation.

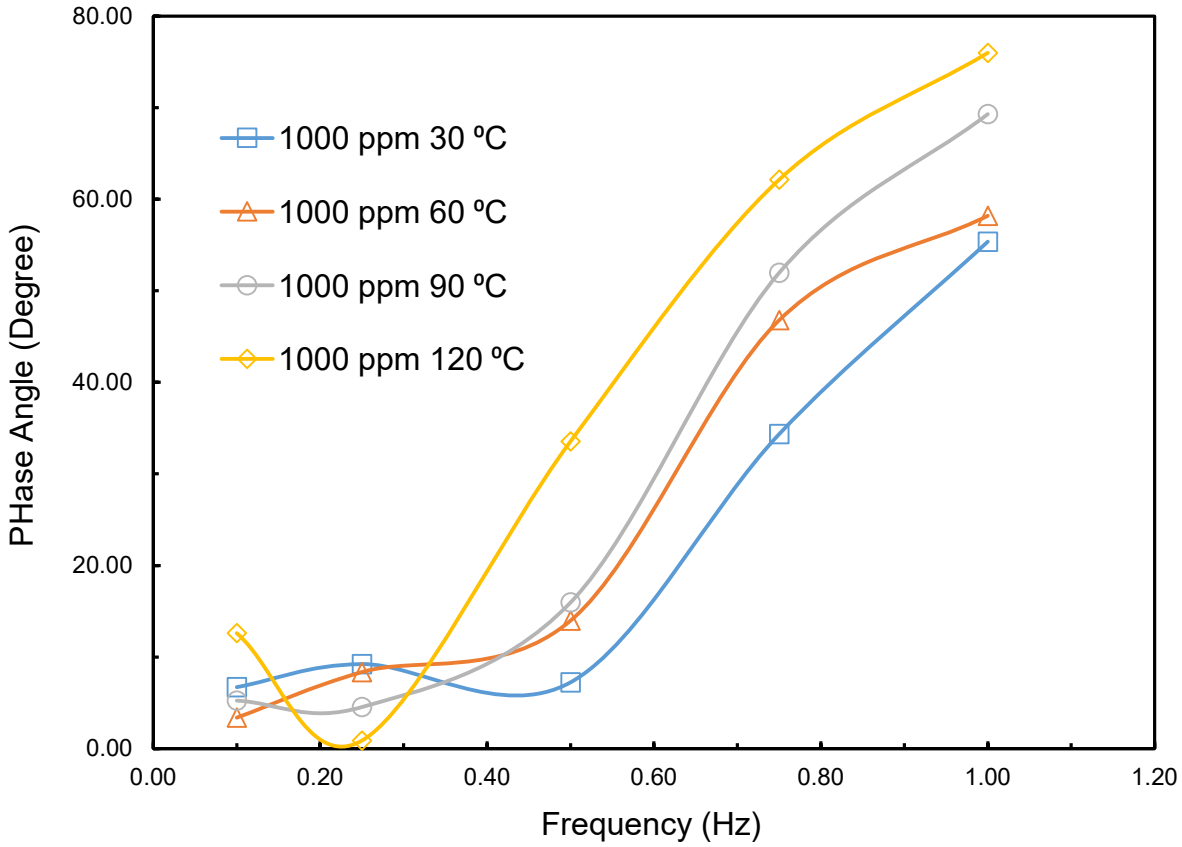

Figure 4. 6 Effect of oscillation frequency on phase angles of 1000 ppm of asphaltenes/toluene pendant drop in water at 30, 60, 90 and 120 °C. The curves are visual aids.

For a demonstration of viscoelastic property, the phase angle shows that as the frequency increases, the phase angle also increases. This is majorly due to the increase in elastic moduli because viscous moduli remain no different with temperature change. As the oscillation frequency increases, the resulting asphaltene films shift from gel state to a liquid state. With increased temperature, more liquid property was observed.

4.4.3 Interfacial Dilatational Rheology of 100, 1000 and 10000 ppm of Asphaltenes in Toluene/Water Interface at 120 °C

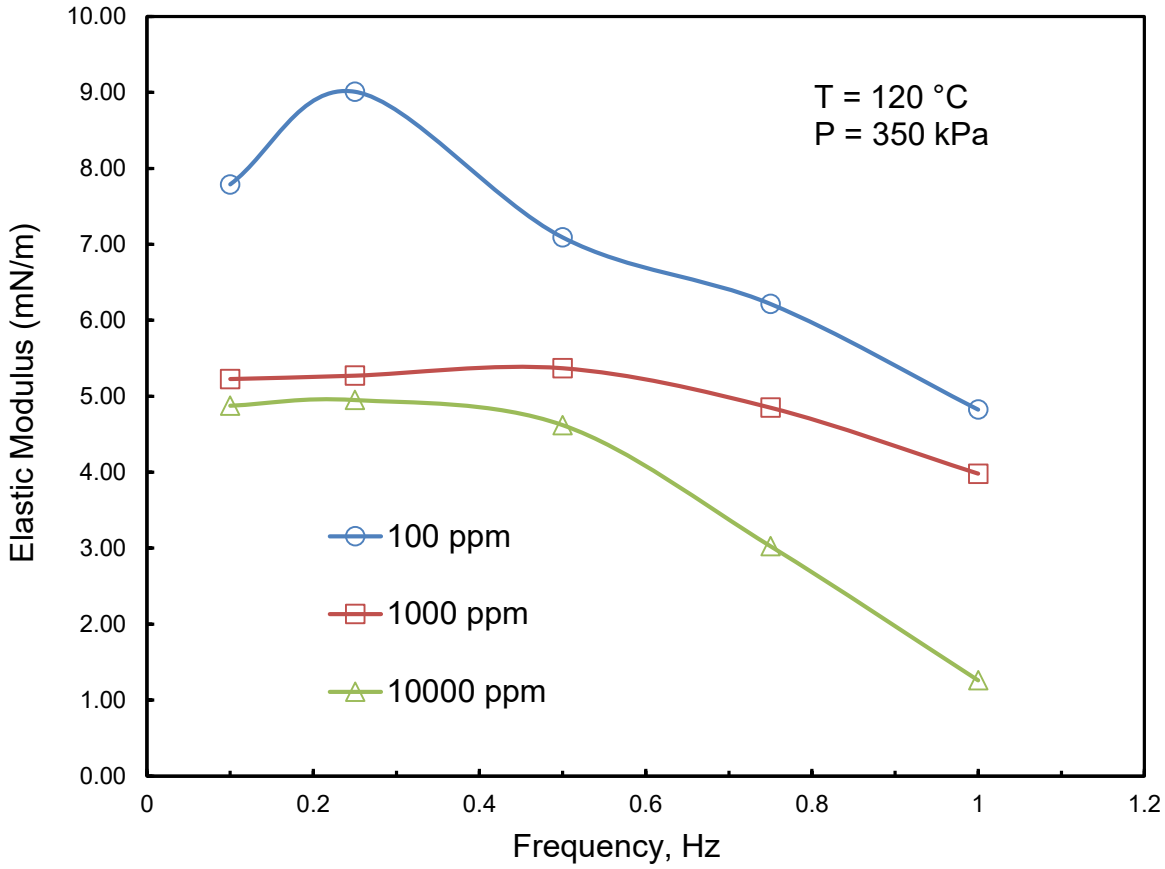

Figure 4. 7 Effect of oscillation frequency on elastic modulus in the system of 100, 1000 and 10000 ppm of asphaltenes in toluene solution at 120 ºC. Curves are visual aids.

For the elastic moduli with different concentration of asphaltenes concentration in toluene at 120 °C, as the concentration increases, the elastic moduli of each curve decrease gradually. As shown in Chapter 3.3.1, as the concentration of the asphaltenes/toluene increases, the diffusion coefficients of asphaltene molecules decrease. However, the highest concentration tried in the previous research was 2000 ppm. Here at 10000 ppm, significant reduction of elastic moduli was observed which indicates more asphaltenes adsorbed at toluene/water interface.

As discussed in Chapter 4.4.1, the elastic moduli may be independent of the oscillation frequency. However, in this subchapter for 10000 ppm of asphaltene solutions, as the frequency increases, the elastic moduli decrease significantly.

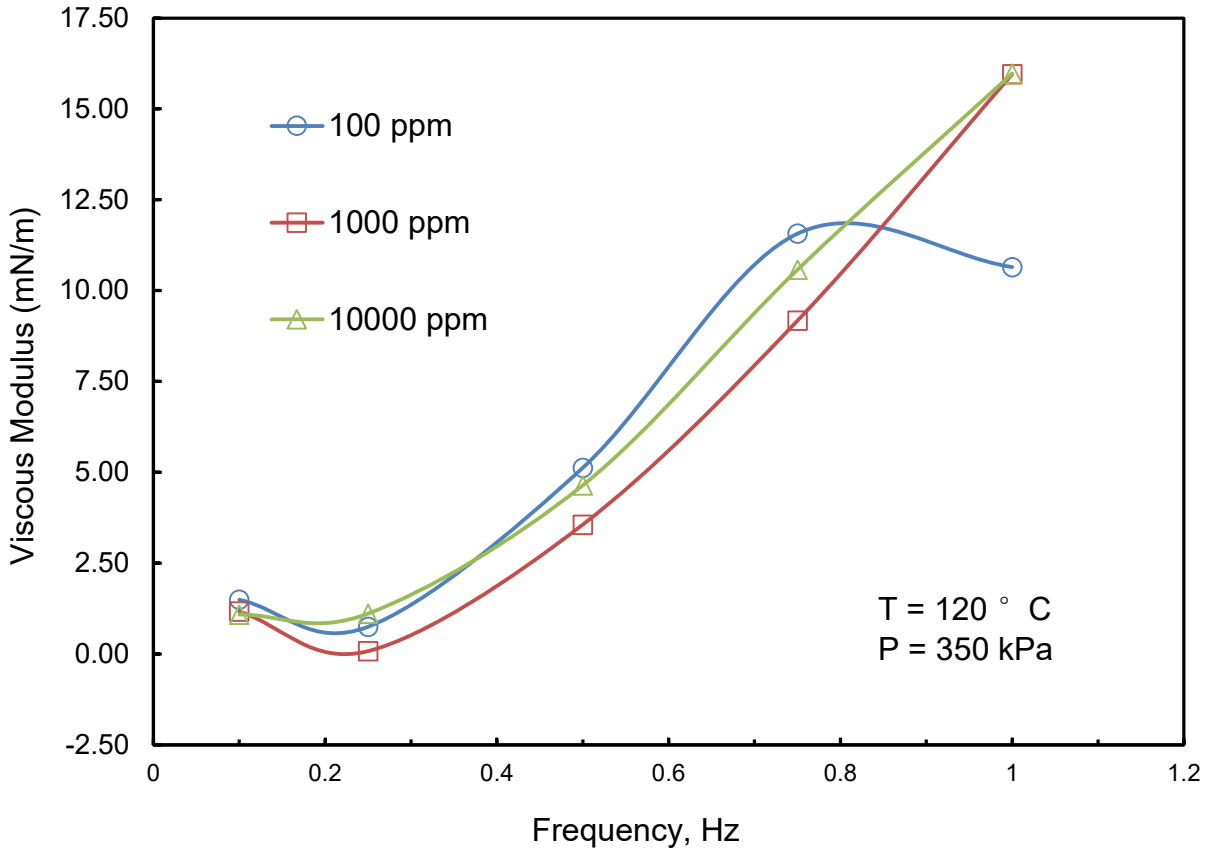

Figure 4. 8 Effect of oscillation frequency on viscous modulus in the system of 100, 1000 and 10000 ppm of asphaltene in toluene solution at 120 ºC. Curves are visual aids.

As the frequency increased from 0.1 to 1.0 Hz, all three viscous moduli increase significantly. However, as the concentration of asphaltenes increases, no major difference was observed. From this result, one can conclude that the viscous moduli are independent of asphaltene concentrations.

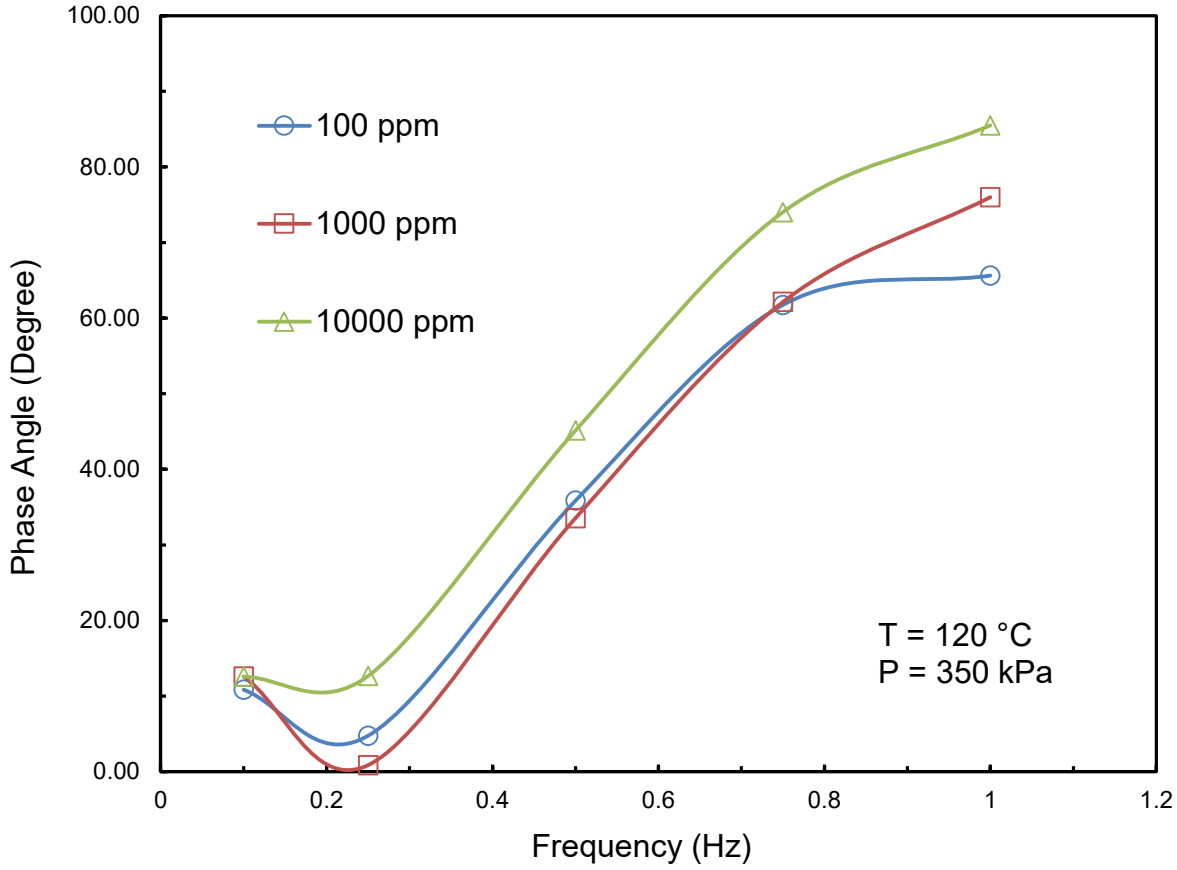

Figure 4. 9 Effect of oscillation frequency on phase angle in the system of 100, 1000 and 10000 ppm of asphaltene in toluene solution at 120 ºC. Curves are visual aids.

For phase angle measurement, as the frequency increases, the phase angle increases to near 90 ° and more liquid properties were displayed for all three curves. Still, the contribution factor is elastic moduli since the viscous moduli do not vary much with concentration. As the concentration of asphaltenes increases, more liquid property was observed for the film formed in the toluene/water interface.

4.4.4 Interfacial Dilatational Rheology of 1000 ppm of Asphaltenes/Toluene Solution in 10, 100 and 500 mM of Sodium Chloride/Water Solution at 120 °C

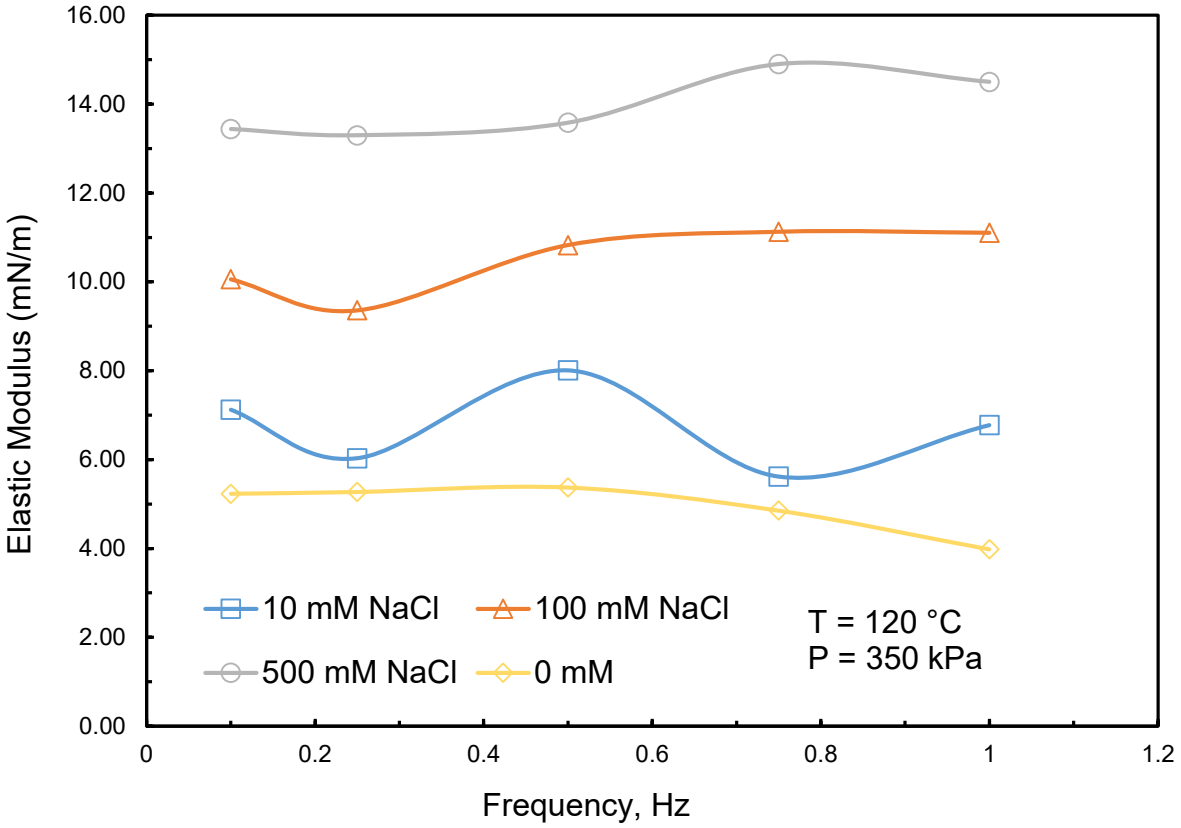

Figure 4. 10 Effect of oscillation frequency on elastic modulus in the system of 1000 ppm of asphaltene in toluene solution with 0, 10, 100, 500 mM of NaCl solution at 120 ºC. Curves are visual aids only.

For this set of study, the sodium chloride solutions were prepared from 10, 100 to 500 mM of concentration. 1000 mM of concentration was also made. However, at higher salt concentration at 120 °C, the brine solution reacted with aluminum pressure vessel with very fast rate. Results cannot be obtained.

Across all frequencies from 0.1 Hz to 1.0 Hz, as the frequency increased, the elastic moduli remain relatively the same level. As the salinity of the aqueous solution increased from 10 to 100 mM of concentration, about 3 mN/m of increase of modulus was observed. Further increased the salt concentration, more increment of elastic moduli was observed. It is suggested that as the salinity of the solution increased, more rigid films were formed between the asphaltenes/toluene solution and water. Therefore, high emulsion stability can be expected.

When inorganic salts are present in the aqueous solution, the water molecules from a cage-like hydrogen bonded structure around the salt ions. At the interface, the salts are depleted near the interface and the surface excess concentration is negative. As predicted by the Gibbs adsorption isotherms with multi components system, interfacial tension increases when surface excess concentration is negative. As the interfacial tension increases, increased elastic moduli is expected.

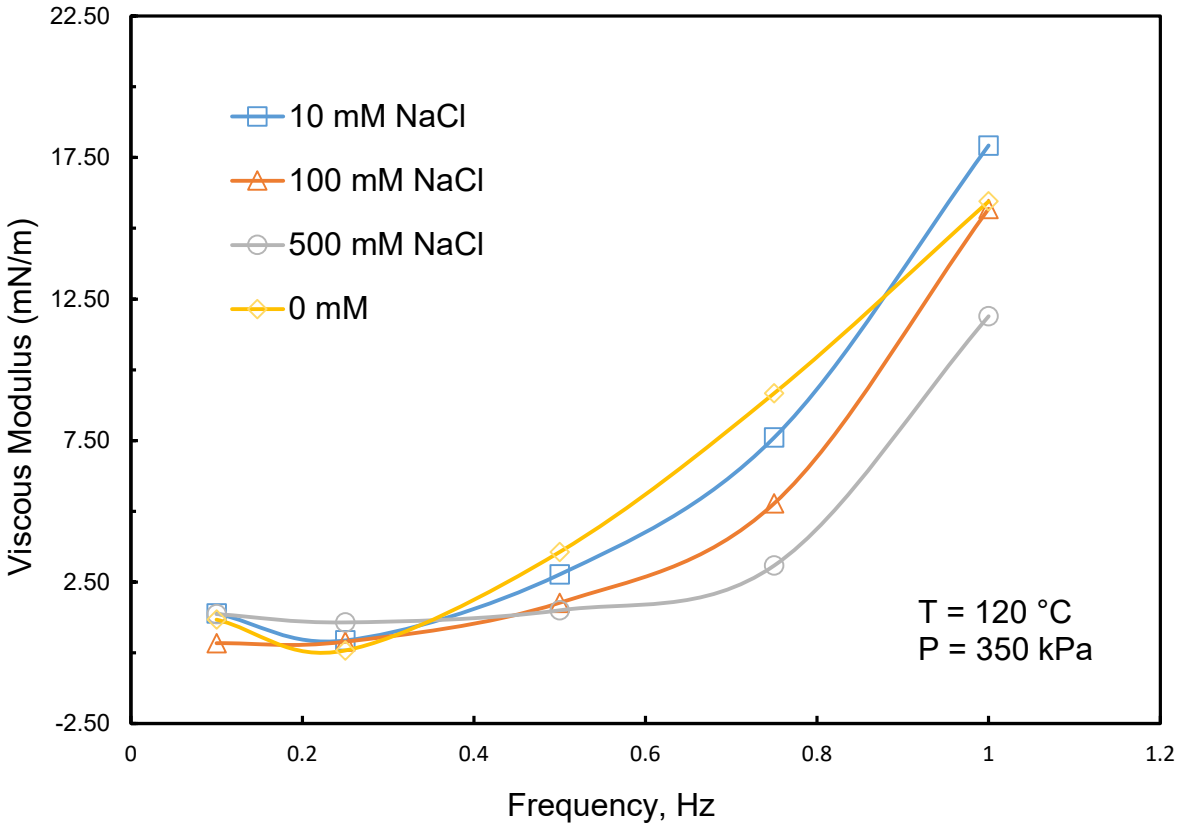

Figure 4. 11 Effect of oscillation frequency on viscous modulus in the system of 1000 ppm of asphaltene in toluene solution with 0, 10, 100, 500 mM of NaCl solution at 120 ºC. Curves are visual aids only.

The general trend has been observed that as the oscillation frequency increases, the viscous moduli increase. With the increase of salinity of brine solution from 10 mM to 500 mM, the viscous moduli decrease gradually. At lower frequencies less than 0.5 Hz, the difference in viscous moduli were insignificant. However, with higher oscillation frequency at 1.0 Hz, 2 mN/m of modulus reduction was observed. As the salt concentration increases, the asphaltene films formed between the toluene and brine solution becomes less liquid-like. Compared to previous Chapter 4.4.2 and 4.4.3,

temperature and asphaltene concentration has little effect on viscous moduli. However, the salt concentration has pronounced effect on viscous moduli of asphaltene in toluene/water system.

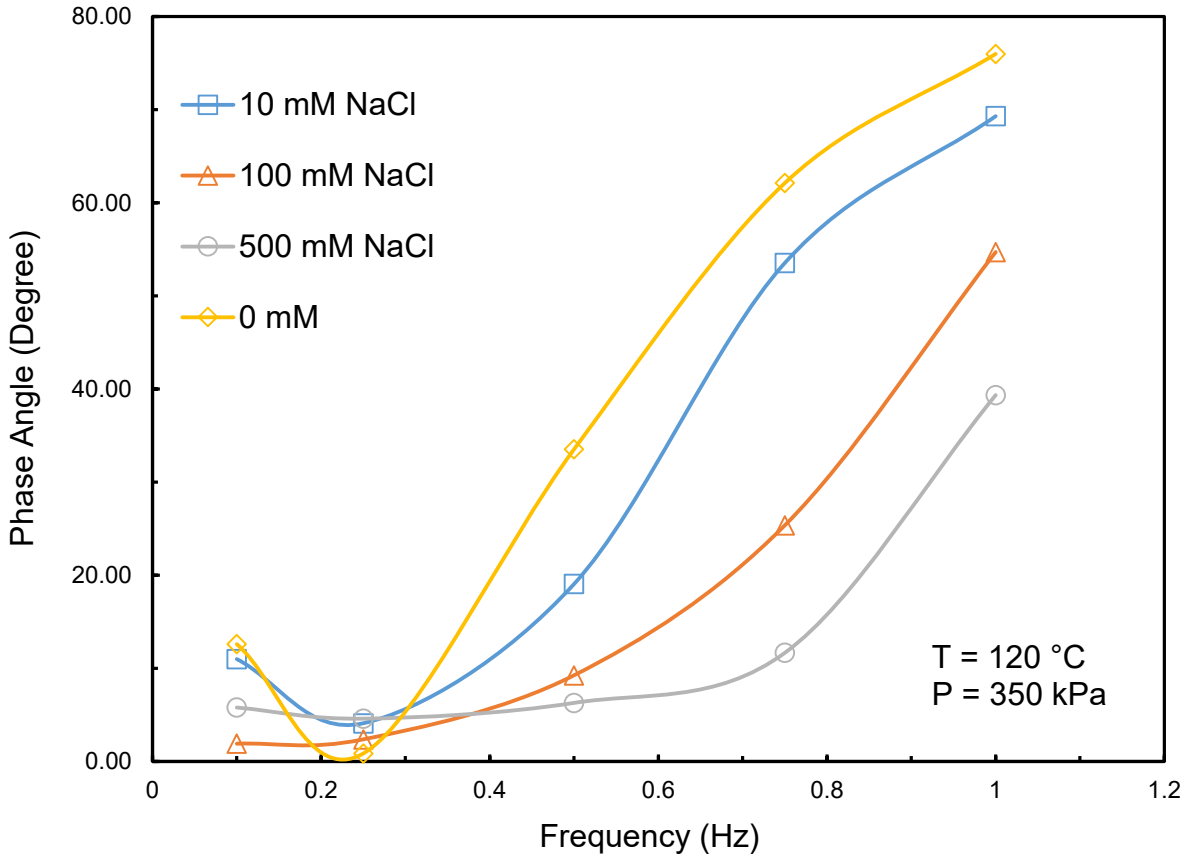

Figure 4. 12 Effect of oscillation frequency on phase angle in the system of 1000 ppm of asphaltene in toluene solution with 0, 10, 100, 500 mM of NaCl solution at 120 ºC. Curves are visual aids only.

For phase angle measurement, as the oscillation frequency increases, the phase angle increases for different salt concentrations. At higher frequencies above 0.5 Hz, the trends are clear: with increased sodium chloride concentration, the phase angle decreases gradually. The phase angle

further confirms that as the salt concentration increases, the asphaltene films in toluene/water interface becomes more rigid resulting high emulsion stability.

4.5 Conclusions

The general trend observed in these series of testing is that as the oscillation frequency increases, the viscous moduli increase. For interfacial dilatational rheology of pure toluene/water system at various temperature from 30 to 120 °C, as the temperature increased, the elastic moduli decrease, and viscous moduli increase. For 1000 ppm of asphaltenes at toluene/water interface, as the temperature increased, the elastic moduli decreased significantly across all frequencies. The rigid glassy asphaltenes films were softened at higher temperature. For viscous moduli, no significant changes were observed with temperature change. For various concentration of asphaltene/toluene solution from 100 ppm to 10000 ppm at 120 °C, as the frequency increased, they have shown decreased in elastic moduli. As the concentration of asphaltenes increased to 10000 ppm, significant reduction in elastic moduli were observed. Little change was observed in viscous moduli with concentration. With the presence of sodium chloride in the aqueous phase, the interfacial dilatational properties were measured. As the salt concentration increased, the elastic moduli increased significantly. Viscous moduli had shown increasing trend as well. Elevated salinity induced the formation of more rigid asphaltene films at the oil/water interface.

Reference

(1) Acosta, E. "Achieving sustainable, optimal SAGD operations." *Journal of Petroleum Technology***,** 62 (11), 24 – 28.

(2) Saniere, A.; Henaut, I.; Argillier, J. "Pipeline transportation of heavy oils, a strategic, economic and technological challenge." *Oil & Gas Science and Technology.* **2004,** 59, 455 – 466.

(3) Mullins, O. C.; Sabbah, H.; Eyssautier, J.; Pomerantz, A. E.; Barre, L.; Andrews, B.; Ruiz-Morales, Y. et al. "Advances in asphaltene science and the Yen-Mullins model." *Energy & Fuels,* ***2012***, 26 (7), 3986 – 4003.

(4) McLean, J. D.; Kilpatrick, P. K. Effects of asphaltene aggregation in model−toluene mixtures on stability of water-in-oil emulsions. *J. Colloid Interface Sci*. **1997**, 196, 23−34.

(5) Rane, Jayant P., David Harbottle, Vincent Pauchard, Alexander Couzis, and Sanjoy Banerjee. "Adsorption Kinetics of Asphaltenes at the Oil–water Interface and Nanoaggregation in the Bulk." *Langmuir* 28, no. 26 (2012): 9986–9995.

(6) Rane, Jayant P., Vincent Pauchard, Alexander Couzis, and Sanjoy Banerjee. "Interfacial Rheology of Asphaltenes at Oil–water Interfaces and Interpretation of the Equation of State." *Langmuir* 29, no. 15 (2013): 4750–4759.

(7) Zarkar, Sharli, Vincent Pauchard, Umer Farooq, Alexander Couzis, and Sanjoy Banerjee. "Interfacial Properties of Asphaltenes at Toluene–water Interfaces." *Langmuir* 31, no. 17 (2015): 4878–4886.

(8) Aske, Narve, Robert Orr, and Johan Sjöblom. "Dilatational Elasticity Moduli of Water–crude Oil Interfaces Using the Oscillating Pendant Drop." *Journal of Dispersion Science and Technology* 23, no. 6 (2002): 809–825.

(9) Sztukowski, Danuta M., and Harvey W. Yarranton. “Rheology of Asphaltene-Toluene/Water Interfaces.” *Langmuir* 21, no. 25 (2005): 11651–11658.

(10) Yarranton, H. W., D. M. Sztukowski, and P. Urrutia. “Effect of Interfacial Rheology on Model Emulsion Coalescence: I. Interfacial Rheology.” *Journal of Colloid and Interface Science* 310, no. 1 (2007): 246–252.

(11) Angle, Chandra W., and Yujuan Hua. “Dilational Interfacial Rheology for Increasingly Deasphalted Bitumens and N-C5 Asphaltenes in Toluene/NaHCO3 Solution.” *Energy & Fuels* 26, no. 10 (2012): 6228–6239.

(12) Sheu, Eric Y., M. Maureen, and D. A. Storm. “Interfacial Properties of Asphaltenes.” *Fuel* 71, no. 11 (1992): 1277–1281.

(13) Sheu, Eric Y., M. Maureen, Dave A. Storm, and Stephen J. DeCanio. “Aggregation and Kinetics of Asphaltenes in Organic Solvents.” *Fuel* 71, no. 3 (1992): 299–302.

(14) Yarranton, Harvey W., Hussein Alboudwarej, and Rajesh Jakher. “Investigation of Asphaltene Association with Vapor Pressure Osmometry and Interfacial Tension Measurements.” *Industrial & Engineering Chemistry Research* 39, no. 8 (2000): 2916–2924

(15) Rogel, E., O. Leon, G. Torres, and J. Espidel. “Aggregation of Asphaltenes in Organic Solvents Using Surface Tension Measurements.” *Fuel* 79, no. 11 (2000): 1389–1394.

(16) Yu, Guangzhe, Kyle Karinshak, Jeff H. Harwell, Brian P. Grady, Andrew Woodside, and Moniraj Ghosh. “Interfacial Behavior and Water Solubility of Various Asphaltenes at High Temperature.” *Colloids and Surfaces A: Physicochemical and Engineering Aspects* 441 (2014): 378–388.

(17) Jeribi, M., B. Almir-Assad, D. Langevin, I. Henaut, and J. F. Argillier. "Adsorption Kinetics of Asphaltenes at Liquid Interfaces." *Journal of Colloid and Interface Science* 256, no. 2 (2002): 268–272.

(18) Yang, Xiaoli, Vincent J. Verruto, and Peter K. Kilpatrick. "Dynamic Asphaltene- Resin Exchange at the Oil/Water Interface: Time-Dependent W/O Emulsion Stability for Asphaltene/Resin Model Oils." *Energy & Fuels* 21, no. 3 (2007): 1343–1349.

(19) Bauget, Fabrice, Dominique Langevin, and Roland Lenormand. "Dynamic Surface Properties of Asphaltenes and Resins at the Oil–air Interface." *Journal of Colloid and Interface Science* 239, no. 2 (2001): 501–508.

(20) Hu, Chuntian, Nicole C. Garcia, Rongzuo Xu, Tran Cao, Andrew Yen, Susan A. Garner, Jose M. Macias, Nikhil Joshi, and Ryan L. Hartman. "Interfacial Properties of Asphaltenes at the Heptol–Brine Interface." *Energy & Fuels* 30, no. 1 (2015): 80–87.

(21) Silva Ramos, Antônio Carlos da, Lilian Haraguchi, Fábio R. Notrispe, Watson Loh, and Rahoma S. Mohamed. "Interfacial and Colloidal Behavior of Asphaltenes Obtained from Brazilian Crude Oils." *Journal of Petroleum Science and Engineering* 32, no. 2 (2001): 201–216.

(22) Nenningsland, Andreas L., Sébastien Simon, and Johan Sjöblom. "Influence of Interfacial Rheological Properties on Stability of Asphaltene-Stabilized Emulsions." *Journal of Dispersion Science and Technology* 35, no. 2 (2014): 231–243.

(23) Sheu, E. Y., D. A. Storm, and M. B. Shields. "Adsorption Kinetics of Asphaltenes at Toluene/Acid Solution Interface." *Fuel* 74, no. 10 (1995): 1475–1479.

(24) Poteau, Sandrine, Jean-François Argillier, Dominique Langevin, Frédéric Pincet, and Eric Perez. "Influence of pH on Stability and Dynamic Properties of Asphaltenes and Other

Amphiphilic Molecules at the Oil- Water Interface." *Energy & Fuels* 19, no. 4 (2005): 1337–1341.

(25) Salager J.L. (1990) The fundamental basis for the action of a chemical dehydratant: Influence of Physical and Chemical formulation on the stability of an emulsion, *Ind. Chem. Eng.* **30**, 103-116.

(26) Langevin D. (2000) Influence of interfacial rheology on foam and emulsion properties, A*dv. Colloid Interfac.* **88**, 209-222.

(27) Kim Y.H., Wasan D.T., Breen P.J. (1995) A study of dynamic interfacial mechanisms for demulsification of water-in-oil emulsions, *Colloid. Surface A* **95**, 235-247.

(28) Bauget F., Langevin D., Lenormand R. (2001) Dynamic Surface Properties of Asphaltenes and Resins at the Oil/Air Interface, *J. Colloid Interf. Sci.* **239**, 501-508.

(29) Bouriat P., El Kerri N., Graciaa A., Lachaise J. (2004) Properties of a Two-Dimensional Asphaltene a Network at the Water-Cyclohexane Interface Deduced from Dynamic Tensiometry, *Langmuir* **20**, 7459-7464.

(30) Dicharry C., Arla D., Sinquin A., Graciaa A., Bouriat P. (2006) Stability of Water/Crude Oil Emulsions based on Interfacial Dilatational Rheology, *J. Colloid Interf. Sci.* **297**, 785-791.

(31) Hannisdal A., Orr R., Sjoblom J. (2007) Viscoelastic Properties of Crude Oil Components at Oil-Water Interfaces. 1: The Effect of Dilution, *J. Disper. Sci. Technol.* **28**, 1.

(32) Freer E.M., Wong H., Radke C.J. (2005) Oscillating drop/bubble tensiometry: effect of viscous forces on the measurement of interfacial tension, *J. Colloid Interf. Sci.* **282**, 128-132.

(33) Freer E.M., Radke C.J. (2004) Relaxation of asphaltenes at the toluene/water interface: Diffusion exchange and surface rearrangement, *J. Adhesion* **80**, 6, 481-496.

(34) Spiecker P.M., Kilpatrick P.K. (2004) Interfacial Rheology of Petroleum Asphaltenes at the Oil-Water Interface, *Langmuir* **20**, 4022-4032.

(35) Acevedo S., Escobar G., Gutierrez L.B., Rivas H., Gutierrez X. (1993) Interfacial Rheological Studies of Extra-Heavy Crude Oils and Asphaltenes: Role of the Dispersion Effect of Resins in the Adsorption of Asphaltenes at the Interface of Water-in-Crude Oil Emulsions, *Colloid. Surface A* **71**, 65-71.

(36) Mohammed R.A., Bailey A.I., Luckham P.F., Taylor S.E. (1994) The Effect of Demulsifiers on the Interfacial Rheology and Emulsion Stability of Water-in-Crude Oil Emulsions, *Colloid. Surface A* **91**, 129-139.

(37) Daniel-David D., Pezron I., Clausse D., Dalmazzone C., Noik C., Komunjer L. (2004) Interfacial properties of a silicone copolymer demulsifier at the air/water interface, *Phys. Chem. Chem. Phys.* **6**, 1570-1574.

(38) Daniel-David D., Pezron I., Clausse D., Dalmazzone C., Noik C., Komunjer L. (2005) Elastic properties of crude oil/water interface in presence of polymeric emulsion breakers, *Colloid. Surface A* **270-271**, 257-262.

(39) Winter H.H., Chambon F. (1986) Analysis of Linear Viscoelasticity of a Crosslinking Polymer at the Gel Point, *J. Rheol.* **30**, 367-382.

(40) Chambon F., Winter H.H. (1987) Linear Viscoelasticity at the Gel Point of a Crosslinking PDMS with Imbalanced Stoichiometry, *J. Rheol.* **31**, 683-697.

(41) Ese M.E., Sjoblom J., Fordedal H., Urdahl O., Ronningsen H.P. (1997) Ageing of Interfacially Active Components and its Effect on Emulsion Stability as Studied by Means

of High Voltage Dielectric Spectroscopy Measurements, *Colloid. Surface A* **123-124**, 225-232.

(42) Freer E.M., Kam Sub Yim, Fuller G.G., Radke C.J. (2004) Shear and dilatational relaxation mechanisms of globular and flexible proteins at the hexadecane/water interface, *Langmuir* **20**, 10159- 10167.

(43) ASTM D6560-17, Standard Test Method for Determination of Asphaltenes (Heptane Insolubles) in Crude Petroleum and Petroleum Products, *ASTM International*, West Conshohocken, PA, 2017

(44) C.G. Quintero, C. Noïk, C. Dalmazzone, J.L. Grossiord. Formation Kinetics and Viscoelastic Properties of Water/Crude Oil Interfacial Films, *Oil & Gas Science and Technology – Rev. IFP,* Vol. 64 (2009), No. 5, pp. 607-616

Chapter 5 Conclusions and Future Works

5.1 Major Conclusions

In this thesis, dynamic IFT and interfacial dilatational rheology under high temperature and high pressure have been conducted for asphaltenes at oil/water interface. Effect of temperature, surfactants and aromaticity of solvent have been studied for the adsorption kinetics of asphaltenes at oil/water interface. For dilatational interfacial study, pure toluene/water system was established as baseline, the effect of temperature, concentration of asphaltenes solutions and effect of salinity in aqueous phase were investigated.

1. For adsorption kinetics, based on the rate of decreasing IFT curves, three regimes can be observed. At each regime, the reduction of IFT was dominated by different process.
2. At Regime I, the reduction of IFT can be fitted into a linear relationship with the square root of time. The relationship agreed with Ward-Tordai model and indicates that Regime I was a diffusion-controlled process. Regime II was a transitional stage where the steric hindrance of adsorbed asphaltenes prevent the continuous diffusion/adsorption of new asphaltenes, leading to reduced decay rate of dynamic IFT. Regime III was the continuous adsorption of asphaltenes to the oil/water interface and reconfiguration of adsorbed asphaltenes. Gibbs adsorption model was used and the equilibrium was reached. The equilibrium IFT was determined by extrapolating the dynamic IFT curve with the inverse square root of time and intercept at Y axis for final equilibrium value.
3. For dynamic IFT vs. time for 1000 ppm of asphaltenes at toluene/water system, with increasing temperature from 30 to 90 °C, the dynamic IFT decreased significantly and the diffusion process accelerated.

4. For dynamic IFT vs. time for 1000 ppm of asphaltenes at toluene/water system with the addition of 25 ppm of PEG-PPG-PEG surfactants, at 30 °C, the addition of surfactants reduces the dynamic IFT with a factor of greater than 3. The diffusion coefficient increased an order of magnitude larger. With the increase of temperature gradually to 60 °C and 90 °C, the decay rate of dynamic IFT decreased compared to that of 30 °C.
5. With increased volume percentage of heptane in solvent system comprised of toluene and heptane, greater reduction of dynamic IFT was found for this asphaltenes sample.
6. For interfacial dilatational rheology measurement, the general trend relating oscillation frequency is that as oscillation frequency increases, viscous moduli and phase angles increase.
7. For interfacial dilatational rheology of toluene/water system at various temperature from 30 to 120 °C, as the temperature increased, the elastic moduli decreased, and viscous moduli increased in general, hence, an increase in phase angle.
8. For 1000 ppm of asphaltenes at toluene/water interface, as the temperature increased, the elastic moduli decreased significantly across all frequencies. The more rigid glassy asphaltenes films were softened at higher temperature. However, for viscous moduli, no significant changes were observed.
9. For various concentration of asphaltene/toluene solution from 100 ppm, 1000 ppm and 10000 ppm at 120 °C, as the frequency increased, they have shown decreased in elastic moduli. As the concentration of asphaltenes increased to 10000 ppm, significant reduction in elastic moduli were observed. Little change was observed in viscous moduli.

10. With the presence of sodium chloride in the aqueous phase, the interfacial dilatational properties were measured. As the concentration increased, the elastic moduli increased significantly as well. Viscous moduli had shown decreasing trend.

5.2 Future Works & Possible Improvement

In this thesis, IFT and dilatational rheology of asphaltene solutions under different conditions have been investigated. To further improve the experiment for better accuracy and capabilities, the following modification and experiments should be performed in the future.

1. The temperature control is crucial for this experiment. The temperature control contains two folds: first, the heating element for current setup is limited to 400 W. To achieve even higher temperature, more wattage is required. The ideal wattage is about 1200 W for 115 V application. For the size of this vessel, it can reach 250 °C with specially made fiber glass insulation.
2. Secondly, the temperature fluctuation should be minimized. This instrument setup uses single loop temperature feedback system. The thermocouple is directly in contact with bulk fluid. However, the heating element and vessel which made of metal conduct the heat slowly creating a delay in temperature sensing. The temperature fluctuation has been observed in the vessel where convection current observed from the camera. To remedy this, a double loop temperature feedback system should be used: one thermocouple feedbacks the temperature of pressure vessel and heating element, and the 2nd thermocouple measured the inside fluid temperature. This allow the heating element limited to certain temperature, and then the fluid catch up the exterior temperature gradually. The best option is to use a liquid circulation bath from renowned manufacture. The liquid circulation bath is

exceptionally keeping the temperature in very close range of 0.01 °C. However, for this application, the circulation pump generates pulsation and vibration could impede the sensitive pendant drop measurement.

3. The material of the pressure vessel should be improved. The current pressure vessel is made of certain grade of aluminum. Aluminum is excellent at conducting heat and being light weight. However, while performing experiment with 100 mM and 500 mM of NaCl at 120 °C, one can observe that the aluminum surface has been etched away by the high temperature brine solution. At 500 mM of NaCl, the reaction rate was fast. Therefore, no higher concentration of brine solution was experimented.
4. Throughout the whole experiment, majority of modification was performed on oscillator. The original manufacture stated that the oscillator should not be used under pressure. However, based on their calculation and design, the oscillator can certainly handle less than 700 kPa of pressure. At lower frequency around 0.1 Hz at 120 °C, the oscillator plunger piston needs to overcome 340 kPa of liquid pressure with very precise movement. One observed that the piston was having trouble to move smoothly and resulting slight intermittent lagging motion. For future works, a piston should be designed to allow both side of the piston to fill with liquid to balance out the liquid pressure. Therefore, a smooth motion can be achieved.
5. High-speed camera and image requisition. The maximum oscillation frequency achieved in this study was 1 Hz. Sometimes, experiments with oscillation frequency higher than 1 Hz can be achieved, however, due to the requisition speed of the camera system, the camera system installed on this goniometer was not able to record the full sinusoidal cycle of the dilatational changes. Due to the intermittent image capture between cycles, erroneous

numbers could be generated. For oscillation frequency of 1 Hz, a minimum of 10 image captures is required to successfully display a sinusoidal wave form, hence a factor of 10. 10 frames per second camera system is required. For higher frequency such as 3 Hz, 30 frames per second frame rate is required. Future high-speed camera or programming required for high oscillation frequency capturing. Higher frequency helps simulate the condition happened in the real system where agitation and fluid velocities are much greater than in laboratory conditions.

6. Chemical Evaluation: More chemistries with different chemical families and structure variations can be tested. Compared to most literatures, the IFT testing were conducted at ambient laboratory temperature. Based on the behavior of the chemical tested in the article, at different temperatures the chemistries may behave very differently.

Bibliography

(1) Acosta, E. "Achieving sustainable, optimal SAGD operations." *Journal of Petroleum Technology*, 62 (11), 24 – 28.

(2) Saniere, A.; Henaut, I.; Argillier, J. "Pipeline transportation of heavy oils, a strategic, economic and technological challenge." *Oil & Gas Science and Technology.* **2004,** 59, 455 – 466.

(3) Wu, X. A.; Czarnecki, J. "Modeling diluted bitumen-water interfacial compositions using a thermodynamic approach." *Energy & Fuels.* **2005,** 19 (4), 1353 – 1359.

(4) McLean, J. D.; Kilpatrick, P.K. "Effect of asphaltene aggregation in model-toluene mixtures on stability of water-in-oil emulsions." *J. Colloid Interface Sci.* **1997**, 196, 23 – 24.

(5) Yarranton, H. W.; Sztukowski, D. M.; Urrutia, P. "Effect of interfacial rheology on model emulsion coalescence: I. Interfacial rheology." *J. Colloid Interface Sci.* **2007**, 310 (1), 246 – 252.

(6) Kilpatrick, P. K. "Water-in-crude oil emulsion stabilization: review and unanswered questions." *Energy & Fuels.* **2012,** 26 (7), 4017 – 4026.

(7) Adams, J. J. "Asphaltene adsorption, a literature review." *Energy & Fuels,* **2014,** 28 (5), 2831 – 2856

(8) Speight, J. G. "*The chemistry and technology of petroleum*." 3rd ed. Marcel Dekker, New York, **1999;** p xiv, 918p

(9) Mullins, O. C. "*Asphaltenes, heavy oils, and petroleomics."* Springer: New York, **2007;** p xxi, 669p

(10) Mullins, O. C.; Sabbah, H.; Eyssautier, J.; Pomerantz, A. E.; Barre, L.; Andrews, B.; Ruiz-Morales, Y. et al. "Advances in asphaltene science and the Yen-Mullins model." *Energy & Fuels, **2012***, 26 (7), 3986 – 4003.

(11) Groenzin, H.; Mullins, O. C. "Molecular size and structure of asphaltenes from various sources." *Energy & Fuels*, **2000**, 14 (3), 677 – 684.

(12) Rogel, E.; Leon, O.; Torres, G.; Espidel, J. "Aggregation of asphaltenes in organic solvents using surface tension measurements." *Fuel,* **2000,** 79 (11), 1389 – 1394.

(13) Masliyah, J. H.; Czarnecki, J. A.; Xu, Z. "*Handbook on theory and practice of bitumen recovery from Athabasca Oil Sands, Vol I and II."* University of Alberta Press, Edmonton, AB, **2011.**

(14) Butt, H.; Graf, K.; Kappl, M. "*Physics and chemistries of interfaces."* Wiley. p. 32.

(15) Sheu, E. Y.; Storm, D. A.; Shields, M. B. "Adsorption kinetics of asphaltenes at toluene/acid solution interface." *Fuel,* **1995**, 74 (10), 1475 – 1479.

(16) Hu, C.; Garcia, N. C.; Xu, R.; Cao, T; Yen, A.; Garner, S. A.; Macias, J. M.; Joshi, N.; Hartman, R. L. "Interfacial properties of asphaltenes at the Heptol-Brine interface." *Energy & Fuels,* **2015,** 30 (1), 80 – 87.

(17) Farooq, U.; Simon, S.; Tweheyo, M. T.; Øye, G.; Sjöblom, J.; "Interfacial tension measurements between oil fractions of a crude oil and aqueous solutions with different ionic composition and pH." *Journal of Dispersion Science and Technology,* **2013**, 34 (5), 701 – 708.

(18) Rane, J. P.; Harbottle, D.; Pauchard, V.; Couzis, A.; Banerjee, S.; "Adsorption kinetics of asphaltenes at oil-water interface and nanoaggregation in the bulk." *Langmuir,* **2012**, 28 (26), 9986 – 9995.

(19) Bouriat, P.; Kerri, N. E.; Graciaa, A.; Lachaise, J.; "Properties of a two-dimensional asphaltene network at the water-cyclohexane interface deduced from dynamic tensiometry." *Langmuir,* **2004**, 20 (18), 7459 – 7464.

(20) Pauchard, V.; Rane, J. P.; Zarkar, S.; Couzis, A.; Banerjee, S.; "Long-term adsorption kinetics of asphaltenes at the oil-water interface: a random sequential adsorption perspective." *Langmuir,* **2014**, 30 (28), 8381 – 8390.

(21) Jennings, H. Y. JR.; "The effect of temperature and pressure on the interfacial tension of benzene-water and normal decane-water." *Journal of colloid and interface science,* **1967,** 24, 323 – 329.

(22) Hu, C.; Garcia, N. C.; Xu, R.; Cao, T.; Yen, A.; Garner, S. A.; Macias, J. M.; Joshi, N.; Hartman, R. L., Interfacial Properties of Asphaltenes at the Heptol–Brine Interface. *Energy & Fuels* **2016,** *30*, 80-87.

(23) Czarnecki, J.; Moran, K., On the stabilization mechanism of water-in-oil emulsions in petroleum systems. *Energy & Fuels* **2005,** *19*, 2074-2079.

(24) He, Kai, Christina Nguyen, Ramya Kothamasu, Liang Xu, and others. "Insights into Whether Low Salinity Brine Enhances Oil Production in Liquids-Rich Shale Formations." *EUROPEC 2015*. Society of Petroleum Engineers, 2015.

(25) Silva Ramos, Antônio Carlos da, Lilian Haraguchi, Fábio R. Notrispe, Watson Loh, and Rahoma S. Mohamed. "Interfacial and Colloidal Behavior of Asphaltenes Obtained from Brazilian Crude Oils." *Journal of Petroleum Science and Engineering* 32, no. 2 (2001): 201–216.

(26) Bos, Martin A., and Ton van Vliet. “Interfacial Rheological Properties of Adsorbed Protein Layers and Surfactants: A Review.” *Advances in Colloid and Interface Science* 91, no. 3 (2001): 437–471.

(27) Nguyen, D.; Balsamo, V.; Phan, J., Effect of Diluents and Asphaltenes on Interfacial Properties and Steam-Assisted Gravity Drainage Emulsion Stability: Interfacial Rheology and Wettability. *Energy & Fuels* **2014,** *28*, 1641-1651.

(28) Aske, Narve, Robert Orr, Johan Sjöblom, Harald Kallevik, and Gisle Øye. “Interfacial Properties of Water–crude Oil Systems Using the Oscillating Pendant Drop Correlations to Asphaltene Solubility by near Infrared Spectroscopy.” *Journal of Dispersion Science and Technology* 25, no. 3 (2004): 263–275.

(29) Zarkar, Sharli, Vincent Pauchard, Umer Farooq, Alexander Couzis, and Sanjoy Banerjee. “Interfacial Properties of Asphaltenes at Toluene–water Interfaces.” *Langmuir* 31, no. 17 (2015): 4878–4886.

(30) Alves, Douglas R., Juliana SA Carneiro, Iago F. Oliveira, Francisco Façanha, Alexandre F. Santos, Claudio Dariva, Elton Franceschi, and Montserrat Fortuny. “Influence of the Salinity on the Interfacial Properties of a Brazilian Crude Oil–brine Systems.” *Fuel* 118 (2014): 21–26.

(31) Kumar, B. Effect of Salinity on the Interfacial Tension of Model and Crude Oil Systems; M.Sc. Thesis; University of Calgary: Alberta, Canada, 2012.

(32) Lisa Mondy, Carlton Brooks, Anne Grillet, Harry Moffat, Tim Koehler, Melissa Yaklin, Matt Reichert, Lynn Walker, Raymond Cote, Jaime Castañeda, Surface Rheology and Interface Stability, SAND2010-7501 Unlimited Release Printed November 2010.

(33) Podgorski, D. C. (2013). "Heavy Petroleum Composition. 5. Compositional and Structural Continuum of Petroleum Revealed". *Energy & Fuels*. 27 (3): 1268–1276. doi:10.1021/ef301737f.

(34) Spiecker, P. M.; Kilpatrick, P. K., Interfacial rheology of petroleum asphaltenes at the oil-water interface. *Langmuir* **2004,** *20*, 4022-4032.

(35) Pauchard, V.; Roy, T., Blockage of coalescence of water droplets in asphaltenes solutions: A jamming perspective. *Colloids and Surfaces A: Physicochemical and Engineering Aspects* **2014,** *443*, 410-417.

(36) Samaniuk, J. R.; Hermans, E.; Verwijlen, T.; Pauchard, V.; Vermant, J., Soft-Glassy Rheology of Asphaltenes at Liquid Interfaces. *Journal of Dispersion Science and Technology* **2015,** *36*, 1444-1451.

(37) ASTM D6560-17, Standard Test Method for Determination of Asphaltenes (Heptane Insolubles) in Crude Petroleum and Petroleum Products, *ASTM International*, West Conshohocken, PA, 2017

(38) Beverung, C. J.; Radke, C. J.; Blanch, H. W., Protein adsorption at the oil/water interface: characterization of adsorption kinetics by dynamic interfacial tension measurements. *Biophys Chem* **1999,** *81*, 59-80.

(39) Sheu, E. Y., Petroleum asphaltene-properties, characterization, and issues. *Energy & Fuels* **2002,** *16*, 74-82.

(40) Li, Z. F.; Geisel, K.; Richtering, W.; Ngai, T., Poly(N-isopropylacrylamide) microgels at the oil-water interface: adsorption kinetics. *Soft Matter* **2013,** *9*, 9939-9946.

(41) Giusti, F.; Popot, J. L.; Tribet, C., Well-defined critical association concentration and rapid adsorption at the air/water interface of a short amphiphilic polymer, amphipol A8-35: a

study by Forster resonance energy transfer and dynamic surface tension measurements. *Langmuir* **2012,** *28*, 10372-80.

(42) Benjamins, J., J. A. De Feijter, M. T. A. Evans, D. E. Graham, and M. C. Phillips., Dynamic and Static Properties of Proteins Adsorbed at the Air/water Interface. *Faraday Discussions of the Chemical Society* **1975**.

(43) Graham, D. E.; Phillips, M. C., Proteins at Liquid Interfaces .1. Kinetics of Adsorption and Surface Denaturation. *Journal of Colloid and Interface Science* **1979,** *70*, 403-414.

(44) Poteau, S.; Argillier, J. F.; Langevin, D.; Pincet, F.; Perez, E., Influence of pH on stability and dynamic properties of asphaltenes and other amphiphilic molecules at the oil-water interface. *Energy & Fuels* **2005,** *19*, 1337-1341.

(45) Yarranton, H. W.; Alboudwarej, H.; Jakher, R., Investigation of asphaltene association with vapor pressure osmometry and interfacial tension measurements. *Industrial & Engineering Chemistry Research* **2000,** *39*, 2916-2924.

(46) Rane, Jayant P., Vincent Pauchard, Alexander Couzis, and Sanjoy Banerjee. "Interfacial Rheology of Asphaltenes at Oil–water Interfaces and Interpretation of the Equation of State." *Langmuir* 29, no. 15 (2013): 4750–4759.

(47) Aske, Narve, Robert Orr, and Johan Sjöblom. "Dilatational Elasticity Moduli of Water–crude Oil Interfaces Using the Oscillating Pendant Drop." *Journal of Dispersion Science and Technology* 23, no. 6 (2002): 809–825.

(48) Sztukowski, Danuta M., and Harvey W. Yarranton. "Rheology of Asphaltene-Toluene/Water Interfaces." *Langmuir* 21, no. 25 (2005): 11651–11658.

(49) Angle, Chandra W., and Yujuan Hua. “Dilational Interfacial Rheology for Increasingly Deasphalted Bitumens and N-C5 Asphaltenes in Toluene/NaHCO3 Solution.” *Energy & Fuels* 26, no. 10 (2012): 6228–6239.

(50) Sheu, Eric Y., M. Maureen, and D. A. Storm. “Interfacial Properties of Asphaltenes.” *Fuel* 71, no. 11 (1992): 1277–1281.

(51) Sheu, Eric Y., M. Maureen, Dave A. Storm, and Stephen J. DeCanio. “Aggregation and Kinetics of Asphaltenes in Organic Solvents.” *Fuel* 71, no. 3 (1992): 299–302.

(52) Yarranton, Harvey W., Hussein Alboudwarej, and Rajesh Jakher. “Investigation of Asphaltene Association with Vapor Pressure Osmometry and Interfacial Tension Measurements.” *Industrial & Engineering Chemistry Research* 39, no. 8 (2000): 2916–2924

(53) Yu, Guangzhe, Kyle Karinshak, Jeff H. Harwell, Brian P. Grady, Andrew Woodside, and Moniraj Ghosh. “Interfacial Behavior and Water Solubility of Various Asphaltenes at High Temperature.” *Colloids and Surfaces A: Physicochemical and Engineering Aspects* 441 (2014): 378–388.

(54) Jeribi, M., B. Almir-Assad, D. Langevin, I. Henaut, and J. F. Argillier. “Adsorption Kinetics of Asphaltenes at Liquid Interfaces.” *Journal of Colloid and Interface Science* 256, no. 2 (2002): 268–272.

(55) Yang, Xiaoli, Vincent J. Verruto, and Peter K. Kilpatrick. “Dynamic Asphaltene- Resin Exchange at the Oil/Water Interface: Time-Dependent W/O Emulsion Stability for Asphaltene/Resin Model Oils.” *Energy & Fuels* 21, no. 3 (2007): 1343–1349.

(56) Bauget, Fabrice, Dominique Langevin, and Roland Lenormand. “Dynamic Surface Properties of Asphaltenes and Resins at the Oil–air Interface.” *Journal of Colloid and Interface Science* 239, no. 2 (2001): 501–508.

(57) Hu, Chuntian, Nicole C. Garcia, Rongzuo Xu, Tran Cao, Andrew Yen, Susan A. Garner, Jose M. Macias, Nikhil Joshi, and Ryan L. Hartman. “Interfacial Properties of Asphaltenes at the Heptol–Brine Interface.” *Energy & Fuels* 30, no. 1 (2015): 80–87.

(58) Nenningsland, Andreas L., Sébastien Simon, and Johan Sjöblom. “Influence of Interfacial Rheological Properties on Stability of Asphaltene-Stabilized Emulsions.” *Journal of Dispersion Science and Technology* 35, no. 2 (2014): 231–243.

(59) Salager J.L. (1990) The fundamental basis for the action of a chemical dehydratant: Influence of Physical and Chemical formulation on the stability of an emulsion, *Ind. Chem. Eng.* **30**, 103-116.

(60) Langevin D. (2000) Influence of interfacial rheology on foam and emulsion properties, A*dv. Colloid Interfac.* **88**, 209-222.

(61) Kim Y.H., Wasan D.T., Breen P.J. (1995) A study of dynamic interfacial mechanisms for demulsification of water-in-oil emulsions, *Colloid. Surface A* **95**, 235-247.

(62) Bauget F., Langevin D., Lenormand R. (2001) Dynamic Surface Properties of Asphaltenes and Resins at the Oil/Air Interface, *J. Colloid Interf. Sci.* **239**, 501-508.

(63) Dicharry C., Arla D., Sinquin A., Graciaa A., Bouriat P. (2006) Stability of Water/Crude Oil Emulsions based on Interfacial Dilatational Rheology, *J. Colloid Interf. Sci.* **297**, 785-791.

(64) Hannisdal A., Orr R., Sjoblom J. (2007) Viscoelastic Properties of Crude Oil Components at Oil-Water Interfaces. 1: The Effect of Dilution, *J. Disper. Sci. Technol.* **28**, 1.

(65) Freer E.M., Wong H., Radke C.J. (2005) Oscillating drop/bubble tensiometry: effect of viscous forces on the measurement of interfacial tension, *J. Colloid Interf. Sci.* **282**, 128-132.

(66) Freer E.M., Radke C.J. (2004) Relaxation of asphaltenes at the toluene/water interface: Diffusion exchange and surface rearrangement, *J. Adhesion* **80**, 6, 481-496.

(67) Spiecker P.M., Kilpatrick P.K. (2004) Interfacial Rheology of Petroleum Asphaltenes at the Oil-Water Interface, *Langmuir* **20**, 4022-4032.

(68) Acevedo S., Escobar G., Gutierrez L.B., Rivas H., Gutierrez X. (1993) Interfacial Rheological Studies of Extra-Heavy Crude Oils and Asphaltenes: Role of the Dispersion Effect of Resins in the Adsorption of Asphaltenes at the Interface of Water-in-Crude Oil Emulsions, *Colloid. Surface A* **71**, 65-71.

(69) Mohammed R.A., Bailey A.I., Luckham P.F., Taylor S.E. (1994) The Effect of Demulsifiers on the Interfacial Rheology and Emulsion Stability of Water-in-Crude Oil Emulsions, *Colloid. Surface A* **91**, 129-139.

(70) Daniel-David D., Pezron I., Clausse D., Dalmazzone C., Noik C., Komunjer L. (2004) Interfacial properties of a silicone copolymer demulsifier at the air/water interface, *Phys. Chem. Chem. Phys.* **6**, 1570-1574.

(71) Daniel-David D., Pezron I., Clausse D., Dalmazzone C., Noik C., Komunjer L. (2005) Elastic properties of crude oil/water interface in presence of polymeric emulsion breakers, *Colloid. Surface A* **270-271**, 257-262.

(72) Winter H.H., Chambon F. (1986) Analysis of Linear Viscoelasticity of a Crosslinking Polymer at the Gel Point, *J. Rheol.* **30**, 367-382.

(73) Chambon F., Winter H.H. (1987) Linear Viscoelasticity at the Gel Point of a Crosslinking PDMS with Imbalanced Stoichiometry, *J. Rheol.* **31**, 683-697.

(74) Ese M.E., Sjoblom J., Fordedal H., Urdahl O., Ronningsen H.P. (1997) Ageing of Interfacially Active Components and its Effect on Emulsion Stability as Studied by Means of High Voltage Dielectric Spectroscopy Measurements, *Colloid. Surface A* **123-124**, 225-232.

(75) Freer E.M., Kam Sub Yim, Fuller G.G., Radke C.J. (2004) Shear and dilatational relaxation mechanisms of globular and flexible proteins at the hexadecane/water interface, *Langmuir* **20**, 10159- 10167.

(76) C.G. Quintero, C. Noïk, C. Dalmazzone, J.L. Grossiord. Formation Kinetics and Viscoelastic Properties of Water/Crude Oil Interfacial Films, *Oil & Gas Science and Technology – Rev. IFP,* Vol. 64 (2009), No. 5, pp. 607-616

(77) Ramé-hart Model 250 F4 series Standard Goniometer with DROPimage Advanced v2.5 Setup and User Guide, updated 3-2011, ramé-hart instrument co.

(78) A Program System for Interfacial Tension and Contact Angle Measurement by Image Analysis, Advanced Edition, Finn Knut Hansen.